A combined use of in situ and satellite-derived observations to characterize surface hydrology and its variability in the Congo River Basin

Benjamin Kitambo, Fabrice Papa, Adrien Paris, Raphael M Tshimanga,
Stephane Calmant, Ayan Santos Fleischmann, Frédéric Frappart, Melanie
Becker, Mohammad J Tourian, Catherine Prigent, et al.

A combined use of in situ and satellite-derived observations to characterize surface hydrology and its variability in the Congo River Basin

Benjamin Kitambo[1,2,3], Fabrice Papa[1,4], Adrien Paris[1,5], Raphael M. Tshimanga[2], Stephane
Calmant[1], Ayan Santos Fleischmann[6], Frederic Frappart[1], Melanie Becker[7], Mohammad J.
Tourian[8], Catherine Prigent[9], Johary Andriambeloson[10]

[1]Laboratoire d'Etudes en Géophysique et Océanographie Spatiales (LEGOS), UMR 5566, CNES/CNRS/IRD/UPS, 14 Avenue Edouard Belin, Toulouse, France.
[2]Congo Basin Water Resources Research Center (CRREBaC) and Department of Natural Resources Management, University of Kinshasa (UNIKIN), Kinshasa, DRC.
[3]Department of Geology, University of Lubumbashi (UNILU), Route Kasapa, Lubumbashi, DRC.
[4]UnB, Universidade de Brasília, Institute of Geosciences, Campus Universitario Darcy Ribeiro, 70910-900 Brasilia (DF), Brazil.
[5]Hydro Matters, 1 Chemin de la Pousaraque, 31460 Le Faget, France.
[6]Instituto de Pesquisas Hidráulicas (IPH), Universidade Federal do Rio Grande do Sul (UFRGS), Porto Alegre, RS, Brasil.
[7]LIENSs/CNRS, UMR 7266, ULR/CNRS, 2 rue Olympe de Gouges, La Rochelle, France
[8]Institute of Geodesy, University of Stuttgart, Germany.
[9]Sorbonne Université, Observatoire de Paris, Université PSL, CNRS, LERMA, Paris, France
[10]Université d'Antananarivo, Madagascar, Institut et Observatoire de Géophysique d'Antananarivo (IOGA), Laboratoire de Géophysique de l'Environnement et de Télédétection (LGET)

Correspondence to: Benjamin Kitambo (benjamin.kitambo@legos.obs-mip.fr)

Abstract. The Congo River Basin (CRB) is the second largest river system in the world, but its hydroclimatic characteristics remain relatively poorly known. Here, we jointly analyze a large record of in situ and satellite-derived observations, including long term time series of Surface Water Height (SWH) from radar altimetry (a total of 2,311 virtual stations) and surface water extent (SWE) from a multi-satellite technique to better characterize CRB surface hydrology and its variability. Firstly, we show that SWH from radar altimetry multi-missions agree well with in situ water stage at various locations, with root mean square deviation varying from 10 cm (with Sentinel-3A) to 75 cm (with European Remote Sensing-2). SWE from multi-satellite observations also shows a good behavior over a ~25-year period against in situ observations from sub-basin to basin scale. Both datasets help to better characterize the large spatial and temporal variability of hydrological patterns across the basin, with SWH exhibiting annual amplitude of more than 5 m in the northern sub-basins while Congo main-stream and Cuvette Centrale tributaries vary in smaller proportions (1.5 m to 4.5 m). Furthermore, SWH and SWE help better illustrate the spatial distribution and different timings of the CRB annual flood dynamic and how each sub-basin and tributary contribute to the hydrological regime at the outlet of the basin (the Brazzaville/Kinshasa station), including its peculiar bi-modal pattern. Across the basin, we jointly use SWH and SWE to estimate time lag and water travel time to reach the Brazzaville/Kinshasa station, ranging from 0-1 month in its vicinity downstream the basin up to 3 months in remote areas and small tributaries. Northern sub-basins and the central Congo region highly contribute to the large peak in December-January while the

southern part of the basin supplies water to both hydrological peaks, in particular to the moderate one in April-May. The results are supported using in situ observations at various locations in the basin. Our results contribute to a better characterization of the hydrological variability in the CRB and represent an unprecedented source of information for hydrological modeling and to study hydrological processes over the region.

45

1 Introduction

The Congo River Basin (CRB) is located in the equatorial region of Africa (Fig. 1). It is the second largest river system in the world, both in terms of drainage area and discharge. The basin covers ~3.7 x 10^6 km² and its mean annual flow rate is of about 40.500 m³ s⁻¹ (Laraque et al., 2009; Laraque et al., 2013). It plays a crucial role in the local, regional

50   and global hydrological and biogeochemical cycles with significant influence on the regional climate variability (Nogherotto et al., 2013; Burnett et al., 2020). CRB is indeed one of the three main convective centers in the Tropics (Hastenrath, 1985) and receives an average annual rainfall of around 1,500 mm yr⁻¹. Additionally, about 45 % of the CRB land area is covered by dense tropical forest (Verhegghen et al., 2012), accounting for ~20 % of the global tropical forest and storing about ~80 billion tons of carbon, equivalent to ~2.5 years of current global anthropogenic

55   emissions (Verhegghen et al., 2012; Dargie et al., 2017; Becker et al., 2018). CRB is also characterized by a large network of rivers, along with extensive floodplains and wetlands, such as in the Lualaba region in the southern east part of the basin and the well-known *Cuvette Centrale* (Fig. 1). CRB rainforest and inland waters therefore strongly contribute to the carbon cycle of the basin (Dargie et al., 2017; Fan et al., 2019; Hastie et al., 2021). Additionally, more than 80 % of the human population within the CRB rely on the basin water resources for their livelihood, and are particularly vulnerable to climate variability and alteration, and to any future changes that would occur in the basin

60   water cycle (Inogwabini, 2020). Increasing evidences suggest that changes in land use practices such as large scale mining, deforestation, pose significant threat to the basin water resources availability, including hydrological, ecological, and geomorphological processes in the basin (Bele et al., 2010; Ingram et al., 2011; Nogherotto et al., 2013; Tshimanga and Hughes, 2012; Plisnier et al., 2018). These environmental alterations urge for a better

65   comprehension of the overall basin hydrology across scales. Surprisingly, despite its major importance, CRB is still one of the least studied river basins in the world (Laraque et al., 2020), and has not attracted as much attention among the scientific communities as, for instance, the Amazon Basin (Alsdorf et al., 2016). Therefore, there is still insufficient knowledge of CRB hydro-climatic characteristics and processes and their spatial-temporal variability. This is sustained by the lack of comprehensive and maintained in situ data networks that keep the basin poorly monitored at

70   large scale, therefore limiting our understanding of the major factors controlling freshwater dynamics at proper space and time scales.

Efforts have been carried out to undertake studies using remote sensing and/or numerical modeling to overcome the lack of observational information in the CRB and better characterize the various components of the hydrological cycle (Rosenqvist and Birkett, 2002; Lee et al., 2011; Becker et al., 2014; Becker et al., 2018; Ndehedehe et al., 2019;

75   Crowhurst et al., 2020; Fatras et al., 2021). For instance, seasonal flooding dynamics, water level variations and vegetation types over CRB were derived from JERS-1 (Rosenqvist and Birkett, 2002) or ALOS-PALSAR SAR data, as well as ICESat and Envisat altimetry (Betbeder et al., 2014; Kim et al., 2017). Bwangoy et al. (2010) and Betbeder

et al. (2014) used combinations of SAR L-band and optical images to characterize the *Cuvette Centrale* land cover. They found that the wetland extent reaches 360,000 km² (*i.e.*, 32 % of the total area). Becker et al. (2014) demonstrated

80   the potential of using radar altimetry water levels from Envisat (140 virtual stations VSs) to classify groups of hydrologically similar catchments in the CRB. Becker et al. (2018) combined information based on Global Inundation Extent from Multi-satellite (GIEMS) (Prigent et al., 2007) and altimetry-derived water levels from Envisat (350 VSs) to estimate surface water storage and analyze its variability over the period 2003-2007. Its mean annual variation was estimated at ~81 ± 24 km³ that accounts for 19 ± 5 % of the annual variations of GRACE-derived total terrestrial water

85   storage. Ndehedehe et al. (2019), using the observed Standardized Precipitation Index (SPI) and the global sea surface temperature, examined the impact of the multi-scale ocean-atmosphere phenomena on hydro-climatic extremes, showing that 40 % of the basin during 1994-2006 was affected by severe multi-year droughts. Recently, Fatras et al. (2021) analyzed the hydrological dynamics of the CRB using inundation extent estimates from the multi-angular and dual polarization passive L-band microwave signal from the Soil Moisture and Ocean Salinity (SMOS) satellite along

90   with precipitation for 2010-2017. The mean flooded area was found to be 2.39 % for the entire basin and the dataset helped to characterize floods and droughts during the last ten years.

In addition to remote sensing observations, hydrological modeling represents a valuable tool to study the CRB water cycle (Tshimanga et al., 2011; Tshimanga and Hughes, 2014; Aloysius and Saiers, 2017; Munzimi et al., 2019; O'Loughlin et al., 2019; Paris et al., 2020; Datok et al., 2020). For example, Tshimanga and Hughes (2014) used a

95   semi-distributed rainfall-runoff model to examine runoff generation processes and the impact of future climate and land use changes on water resources availability. The magnitude and timing of high and low flows were adequately captured, with nevertheless an additional wetland sub-model component that was added to the main model to account for wetland and natural reservoirs processes in the basin. Aloysius and Saiers (2017) simulated the variability of runoff in the near future (2016-2035) and mid-century (2046-2065), using a hydrological model forced with precipitation

100   and temperature projections from 25 Global Climate Models (GCMs) under two scenarios of greenhouse gas emission. Munzimi et al. (2019) applied the Geospatial Streamflow Model (GeoSFM) coupled to remotely sensed data to estimate daily river discharge over the basin from 1998 to 2012, revealing a good agreement with the observed flow but also discrepancy in some part of the basin where wetland and lake processes are predominant. O'Loughlin et al. (2019) forced the large-scale LISFLOOD-FP hydraulic model with combined in situ and modelled discharges to

105   understand the Congo River unique bimodal flood pulse. The model was set for the area between Kisangani and Kinshasa on the main stem including major tributaries and the *Cuvette Centrale*. The results revealed that the bimodal annual pattern is predominantly a hydrological rather than hydraulically controlled feature. Paris et al. (2020) demonstrated the possibility of monitoring the hydrological variables in near real time using the hydrologic-hydrodynamic model MGB (Portuguese acronym for large basin model) coupled to the current operational satellite

110   altimetry constellation. The model outputs showed a good consistency with the small number of available observations, yet with some notable inconsistency in the mostly ungauged *Cuvette Centrale* and in the southeastern lakes sub-basins. Datok et al. (2020) used the Soil and Water Assessment Tool model (SWAT) to understand the role of the *Cuvette Centrale* in water resources and ecological services. Their findings have highlighted the important

regulatory function of the *Cuvette Centrale* which receives contributions from the upstream Congo River (33 %),
115 effective precipitation inside the *Cuvette Centrale* (31 %), and other tributaries (36 %).

Most of the above studies based on remote sensing (RS) and hydrological modelling were validated or evaluated against information from others hydrological RS data and/or a few historical gauge data, often enabling only comparisons of seasonal signals (Becker et al., 2018), which also did not cover the same period of data availability (Paris et al., 2020). Therefore, the large size of the basin, its spatial heterogeneity and the lack of in situ observations
120 have made difficult the validation of long-term satellite-derived observations of surface hydrology components and the proper set-up of large-scale hydrological models (Munzimi et al., 2019). Recent results call for the need of a comprehensive spatial coverage of CRB water surface elevation using satellite altimetry-derived observation to encompass the full range of variability across its rivers and wetlands up to its outlet (Carr et al., 2019). Additionally, even if recent efforts have been characterizing how water flows across the CRB, the basin-scale dynamics is still
125 understudied, especially regarding the contributions of the different sub-basins to the entire basin hydrology (Alsdorf et al., 2016; Laraque et al., 2020) and to the annual bimodal pattern in the CRB river discharge near to its mouth. Up to now, only few studies have examined the various contributions and the water transfer from upstream to downstream the basin based on few in situ discharge gauge records (Bricquet, 1993; Laraque et al., 2020) and large-scale modeling (Paris et al., 2020).

130 The aim of this study is therefore twofold. First, we provide for the very first time an intensive and comprehensive validation of long-term remote sensing derived products over the entire CRB, in particular radar altimetry water levels variations (a total of 2,311 VSs over the period of 1995 to 2020) and surface water extent from multi-satellite techniques from 1992 to 2015 (Global Inundation Extent from Multi-satellite, GIEMS-2; Prigent et al., 2020), using an unprecedented in situ database (28 gauges of river discharge and height) containing historical and current records
135 of river flows and stages across the CRB. Next, these long-term observations are used to analyze the spatio-temporal dynamics of the water propagation at sub-basin and basin scale levels, significantly improving our understanding of surface waters dynamics in the CRB.

The paper is organized as follows. Section 2 provides a brief description of the CRB. The data and the method employed in this study are described in section 3. The results are presented in section 4 with the validation and
140 evaluation of satellite-derived products, their characteristics, and their use to understand the spatio-temporal variability of surface water in the CRB. Finally, the conclusions and perspectives are provided in section 5.

2 Study region

The CRB (Fig. 1) is a transboundary basin that encompasses nine riparian countries: Zambia, Tanzania, Rwanda,
145 Burundi, Republic of Congo, Central Africa Republic, Cameroon, Democratic Republic of the Congo (DRC) and Angola. The Congo River starts its course in the southeast of DRC in the village of Musofi (Laraque et al., 2020), then flows through a series of marshy lakes (e.g., Kabwe, Kabele, Upemba, Kisale) to form the Lualaba River. The latter is joined northwest by the Luvua River draining Lake Mweru (Runge, 2007). The river name becomes Congo (formerly Zaire River) from Kisangani until it reaches the ocean. The Kasai River in the southern part (left bank), and
150 the Ubangi and Sangha Rivers from the north (right bank), are the principal tributaries of the Congo River. Other

major tributaries are Lulonga, Ruki on the left bank and Aruwimi on the right bank. In the heart of CRB, stands the *Cuvette Centrale,* a large wetland along the equator (Fig. 1) that plays a crucial role on local and regional hydrologic and carbon cycles. Upstream of Brazzaville/Kinshasa, the Congo River main stem flows through a wide multi-channel reach dominated by several sand bars called Malebo Pool.

155 With a mean annual flow of 40,500 m^3 s^{-1} computed at the Brazzaville/Kinshasa hydrological station from 1902 to 2019 and a basin size of ~3.7 x 10^6 km^2, the equatorial CRB (Fig. 1) stands as the second largest river system worldwide, behind the Amazon River, and the second in length in Africa after the Nile River (Laraque et al., 2020). The CRB is characterized by the hydrological regularity of its regime. Alsdorf et al. (2016), referring to historical studies, report that the annual potential evapotranspiration varies little across the basin from 1,100 to 1,200 mm yr^{-1}.

160 The mean annual rainfall in the central parts of the basin accounts for about 2,000 mm yr^{-1}, decreasing both northward and southward to around 1,100 mm yr^{-1}. The mean temperature is estimated to be about 25 °C.

The topography and vegetation of the basin are generally concentrically distributed all around the *Cuvette Centrale,* bordered by plateaus and mountain ranges (e.g., Mayombe, Chaillu, Batéké). In the center of the basin stands the great equatorial forest with multiple facies surrounded by wooded and grassy savannas, typical of Sudanese climate

165 (Bricquet, 1993; Laraque et al., 2020). In this study, six major sub-basins are considered based on the physiography of the CRB (Fig. 1). These are Lualaba (Southeast), Middle-Congo (center), Ubangui (Northeast), Sangha (Northwest), Kasaï (South-center) and Lower-Congo (Southwest).

3 Data and method

3.1 In situ data

170

Hydrological monitoring in the CRB can be traced back since the year 1903, with the implementation of the Kinshasa gauging site. Until the end of 1960, which marks the end of the colonial era for many riparian countries in the basin, more than 400 gauging sites were installed throughout the CRB to provide water level and discharge data (Tshimanga, 2021). It is unfortunate that many of these data could not be accessible to the public interested in hydrological research

175 and water resources management. Since then, there has been a critical decline of the monitoring network, so that, currently, there are no more than 15 gauges considered as operational (Alsdorf et al., 2016; Laraque et al., 2020). Yet the latest observations are in general not available to the scientific community. Initiatives such as Congo HYdrological Cycle Observing System (Congo-HYCOS) have been carried out to build capacity to collect data and produce consistent and reliable information on CRB hydrological cycle (OMM, 2010).

180 For the present study, we had access to a set of historical and contemporary observations of river water stage (WS) and discharge (Table 1). Those were obtained thanks to the collaboration with the regional partners of the Congo Basin Water Resources Research Center (CRREBaC) and from the Environmental Observation and Research project (ORE HYBAM, https://hybam.obs-mip.fr/fr/website-under-development-2/, last access: 15 February 2021) observational network, and from the Global Runoff Data Centre database (GRDC,

185 https://www.bafg.de/GRDC/EN/02_srvcs/21_tmsrs/210_prtl/prtl_node.html, last access: 02 April 2021). It is worth noting that the discharge data from gauges are generally derived from water level measurements converted into

Hydrology and
Earth System
Sciences

Open Access

EGU

Discussions

discharge using stage-discharge relationships (rating curves). Many of the rating curves related to historical gauges were first calibrated in the early 50's, and no information is available on recent rating curves updates neither regarding their uncertainty despite recent efforts from the the ORE-Hybam program and the Congo-Hydrological Cycle

190 Observing System (HYCOS) program from the World Meteorological Organization (WMO) (Alsdorf et al., 2016). Table 1 is organized in two categories: one with stations providing contemporary observations, i.e., covering a period of time that presents a long overlap (several years) with the satellite era (1995 in our study), and another with stations providing long-term historical observations before the 1990's. In the frame of the Commission Internationale du bassin du Congo-Ubangui-Sangha (CICOS)/CNES/IRD/AFD spatial hydrology working group, the Maluku-Trechot and

195 Mbata hydrometric stations were set-up right under Sentinel-3A (see further) ground-tracks. Additionally, for Kutu-muke, water stages are referenced to an ellipsoid therefore providing surface water elevation.

3.2 Radar altimetry-derived surface water height

Radar altimeters onboard satellites were initially designed to measure the ocean surface topography by providing along-track nadir measurements of water surface elevation (Stammer and Cazenave, 2017). Since the 1990's', radar

200 altimeter observations have also been used for continental hydrology studies and to provide a systematic monitoring of water levels of large rivers, lakes, wetlands and floodplains (Cretaux et al., 2017).
The intersection of the satellite ground track with a water body defines a virtual station (VS) where Surface Water Height (SWH) can be retrieved with a temporal interval sampling provided by the repeat cycle of the orbit (Frappart et al., 2006; Da Silva et al., 2010; Crétaux et al., 2017).

205 The in-depth assessment and validation of the water levels derived from the satellite altimeter over rivers and inland water bodies were performed over different river basins against in situ gauges (Frappart et al., 2006; Seyler et al., 2008; Santos et al., 2010; Papa et al., 2010; Papa et al., 2015; Kao et al., 2019; Kittel et al., 2021; Paris et al., 2020), with satisfactory results and uncertainties ranging between few centimeters to tens of centimeters depending on the environments. Therefore, the stages of continental water retrieved from satellite altimetry have been used for many

210 scientific studies and applications, such as the monitoring of abandoned basins (Andriabeloson et al., 2020), the determination of rating curves in poorly gauged basin for river discharge estimation (Paris et al., 2016; Zakharova et al., 2020), the estimation of the spatio-temporal variations of the surface water storage (Papa et al., 2015; Becker et al., 2018), the connectivity between wetlands, floodplains and river (Park, 2020), and the calibration/validation of hydrological (Sun et al., 2012; Paiva et al., 2013; Corbari et al., 2019) and hydrodynamic (Garambois et al., 2017;

215 Pujol et al., 2020) models.
The satellite altimetry data used in this study were acquired from (1) the European Remote Sensing-2 satellite (ERS-2, providing observations from April 1995 to June 2003 with a 35-day repeat cycle), (2) the Environmental Satellite (ENVISAT, named hereafter ENV, providing observations from March 2002 to June 2012 on the same orbit as ERS-2), (3) Jason-2 and 3 (named hereafter J2 and J3, flying on the same orbit with a 10-day repeat cycle, covering June

220 2008 to October 2019 for J2 and January 2016 to present for J3), (4) the Satellite with ARgos and ALtika (SARAL/Altika, named hereafter SRL, from which we use observations from February 2013 to July 2016 ensuring the continuity of the ERS-2/ENV long-term records on the orbit with 35-day repeat cycle), and (5) Sentinel-3A and

3B missions (named hereafter S3A and S3B, available respectively since February 2016 and April 2018 with a ~27-day repeat cycle). While ERS-2, ENV, SRL, and J2 missions are past missions, J3 and S3A/B are still ongoing

225 missions. The VSs used in this study were either directly downloaded from the global operational database Hydroweb (http://hydroweb.theia-land.fr, last access: 12 May 2021) or processed manually using MAPS (Frappart et al., 2015) and ALTIS softwares (respectively Multi-mission Altimetry Processing Software and Altimetric Time Series Software) and GDR (Geophysical Data Records) provided freely by the CTOH (Center for Topographic studies of the Oceans and Hydrosphere, http://ctoh.legos.obs-mip.fr/, last access: 04 January 2021). We thus reached a total number

230 of 323 VSs from ERS-2, 364 and 342 VSs for ENV and ENV2 (new orbit of ENVISAT since late 2010) respectively, 146 and 98 VSs for J2 and J3 respectively, 358 VSs for SRL, 354 VSs for S3A and 326 VSs for S3B (Fig. 2).

Figure 2d shows the actual combination of VSs derived from different satellite missions with a purpose of generating long-term water levels time series spatialized over the CRB. 25 years, 20 years, 14 years, and 12 years of records were aggregated respectively with ERS-2_ENV_SRL_S3A, ERS-2_ENV_SRL, ENV_SRL and finally J2_J3. The pooling

235 of VSs is based on the principle of the nearest neighbor located at a minimum distance of 2 km (Da Silva et al., 2010; Crétaux et al., 2017).

Height of the reflecting water body derived of processing radar echoes are subject to biases. The biases vary with the algorithm used to process the echo, so called the retracking algorithm, and with the mission (e.g., orbit errors, onboard system, mean error in propagation velocity through atmosphere). Therefore, it is required that these biases are removed

240 in order to compose multi-mission series. We used the set of absolute and inter-mission biases determined at Parintins on the Amazon River, Brazil (D. M. Moreira, personal communication, 2020). At Parintins, the orbits of all the past and present altimetry missions (except S3B) have a ground track in close vicinity of the gauge. The gauge has been surveyed by a ten of static and cinematic GNSS campaigns, giving the ellipsoidal height of the gauge zero and the slope of the water surface. We also took in account for the crustal deflection produced by the hydrological load using

245 the rule given by Moreira et al. (2016). Therefore, all the altimetry measurements could be compared rigorously to the absolute reference provided by the gauge readings, making possible the determination of the biases for each mission and for each retracking algorithm. It is worth noting that this methodology does not take into account possible local or regional phenomena that could have an impact on biases values. Ideally, similar studies should be carried out at several locations on earth to verify whether such regional phenomenon exist or not.

250 Note that there is no common height reference between altimeter-derived water height (referenced to a geoid model) and the in situ water stage (i.e., the altitude of the zero of the gauges is unknown). Therefore, when we want to compare them, we merged them in a same reference by calculating the difference of the averages over the same period and adding this difference to the in situ water stage.

255 ### 3.3 Multi-satellite derived surface water extent

The Global Inundation Extent from Multi-Satellite (GIEMS) captures the spatial and temporal dynamics of the extent of episodic and seasonal inundation, wetlands, rivers, lakes, and irrigated agriculture, at the global scale (Prigent et al., 2001, 2007, 2020) It is developed from complementary multiple-satellite observations (Prigent et al., 2001, 2007;

Papa et al., 2010). The multi-sensor technique to estimate the surface water extent and dynamics is primarily based

260 on passive microwave observations (19 and 85 GHz or 1.58 cm to 0.35 cm in wavelength) from the Special Sensor Microwave/Imager (SSM/I and SSMIS). It also integrates climatologies from visible (0.58-0.68 µm) and near-infrared (0.73-1.1 µm) reflectance and the derived Normalized Difference Vegetation Index (NDVI) from the Advanced Very High-Resolution Radiometer (AVHRR) and active microwaves observations (at 5.25 GHz or 5.71 cm in wavelength) from the ERS scatterometer (Papa et al., 2010). The current data set, called GIEMS-2, estimates the monthly surface

265 water extent at the global scale from 1992 to 2015 on an equal area grid of 0.25° x 0.25° resolution at the equator (i.e., each pixel covers 773 km^2). For more details on the GIEMS-2 technique, we refer to Prigent et al. (2007) and especially Prigent et al. (2020) regarding the latest updates on the estimations of the passive microwave emissivity calculation and the newly quantification of the surface water fraction at pixel level.

The seasonal and interannual dynamics of both the initial and the ~25-year surface water extent have been assessed in

270 different environments against multiple variables such as in situ and altimeter-derived water levels in wetlands, lakes, rivers, in situ river discharges, satellite-derived precipitation or total water storage from Gravity Recovery and Climate Experiment (GRACE) (Prigent et al., 2007; Papa et al., 2010; Papa et al., 2008; Papa et al., 2013, Prigent et al., 2020). GIEMS has been used in different hydrological and climatic applications such as methane surface emission (Ringeval et al., 2010), estimation of the spatio-temporal variations of surface water storage (Frappart et al., 2010; Papa et al.,

275 2013; Papa et al., 2015; Frappart et al., 2015; Becker et al., 2018) and validation of the river flooding scheme at the global scale (Decharme et al., 2008; Decharme et al., 2011).

GIEMS-2 uncertainties are quantified to be about 10 % (Prigent et al., 2007) and generally underestimate small surface water extent (Prigent et al., 2007; Becker et al., 2018). Large freshwater bodies worldwide such as the Lake Baikal, the Great Lakes, Lake Victoria are masked in GIEMS-2. In the CRB, this is the case for Lake Tanganyika (Prigent et

280 al., 2007). This will impact the total extent of surface water at basin-scale, but not its relative variations, as the extent of Lake Tanganyika itself shows small variations on seasonal and interannual timescales.

4 Results

4.1 Validation of satellite surface hydrology datasets and their characteristics in the CRB

4.1.1 Validation of altimetry-derived surface water height

285

Observations of in situ WS (Fig. 1 for their locations, Table 1) over the CRB are compared to radar altimetry SWH (Fig. 3). The comparisons at nine locations cover five sub-basins, including Sangha (Ouesso station, Fig. 3a), Ubangui (Bangui and Mbata stations, Fig. 3d and y), Lualaba (Kisangani and Kindu station, Fig. 3j and p), Kasaï (Kutu-muke

290 and Lumbu-dima, Fig. 3m and g), and Lower-Congo (Brazzaville/Kinshasa and Maluku-Trechot stations, Fig. 3s and v). In order to evaluate the performance of the different satellite missions, we choose the nearest VSs located in the direct vicinity of the different gauges.

Figure 3 -left panel- provides the comparison of SWH time series at the nine gauging stations. It generally shows a very good agreement presenting a similar behavior in the peak-to-peak height variations, within a large set of hydraulic

295 regimes (low and high flow seasons). Similar results in CRB were found by Paris et al. (2020) where the comparisons

were done at seasonal time scale with few tens of centimeters of standard error. Note that the VSs of different missions were not located at the same distance from the in situ gauges (distance ranges between 1 km and 38 km). The gauge is considered right below the satellite track when its distance is less than 2 km, as reported by Da Silva et al. (2010). This can explain some discrepancies generally observed for the VSs far away from the in situ gauges (distance >10

300   km, Fig. 3a). Such discrepancies can be due to severe changes in the cross section between the gauge and the VS, such as changes in river width. For Ouesso (Fig. 3a), ENV2 overestimates the lower water level as compared to the other missions. Fig. 3j, m, p present the benefit of spatial altimetry to complete actual temporal gaps of the in situ observations. Nevertheless, for Kindu (Fig. 3p) ENV and J2 are showing different amplitudes. The difference between radar altimetry water levels and in situ observations (Fig. 3 -center panel-) shows values of the order of few ten

305   centimeters (concentration of points around zero in the histograms). The scatter plots between altimetry -derived SWH and in situ water stage presented in Fig. 3 -right panel- confirm the good relationship observed in the time series. The correlation coefficient ranges between 0.84 and 0.99 with the average standard error of the overall entire series varying from 0.10 m to 0.46 m. The values of Root Mean Square Deviation (RMSD) are found comparable to others obtained in other basins over the world (Leon et al., 2006; Da Silva et al., 2010; Papa et al., 2012; Kittel et al., 2021). The

310   results obtained from the analysis for each satellite mission at each station are summarized in Table 2.

The highest RMSD is 0.66 m at Brazzaville station on the main stem of Congo River related to ERS-2 mission (Table 2) and the lowest values of RMSD is 0.10 m at Mbata station on the Lobaye river with S3A mission (Fig. 3y). The pattern observed in Table 2 is that the RMSD decreases continuously from ERS-2 to S3A. In general, ERS-2 presents larger values of RMSD (above 40 cm) than its successor ENV and lowest coefficient correlation (r) than other satellite

315   missions.

These results are in good accordance with Bogning et al. (2018) and Normandin et al. (2018) which observed that the slight decrease in performances of ERS-2 against ENV can be attributed to the lowest chirp bandwidth acquisition mode which degrades the range resolution. The increasing performance with time (from ERS-2 to S3A) is linked to the mode of acquisition of data from the satellite sensor. ERS-2, ENV, J2/3 and SRL operate in Low Resolution Mode

320   (LRM) with a large ground footprint, while S3A/B (like other missions such as Cryosat-2) uses the Synthetic Aperture Radar (SAR mode) also known as Delay-Doppler Altimetry with a small ground spot (Raney, 1998), resulting in a better spatial resolution than the LRM missions along the track, and thus a better performance. SRL operating at Ka band (smaller footprint) and at a higher sampling frequency also shows good performances as already reported (Bogning et al., 2018; Bonnefond et al., 2018; Normandin et al., 2018). As mentioned above the accuracy of SWH

325   depends on several factors among them the width and the morphology of the river. For instance, at the Bangui station on the Ubangui River, S3B surprisingly presents a RMSD of 0.42 m which is much higher than expected. This can be explained by, amongst others, the fact that its ground track intersects the river in a very oblique way over a large distance (~3 km) and at a location where the section presents several sandbanks, thus impacting the return signal and resulting in less accurate estimates.

330   These validations of radar altimetry SWH in six sub-basins of the CRB provide confidence to use the large sets of VSs to characterize the hydrological dynamics of SWH across the basin. Figure 4a provides a representation of the mean maximal amplitude of SWH at each one of those VSs. The Ubangui and Sangha Rivers in the northern part of

the basin present the largest amplitude variations, up to more than 5 m, while Congo main stem and *Cuvette Centrale*
tributaries vary in smaller proportions (1.5 m to 4.5 m). This finding aligns with previous amplitude values reported
335   in the main stem of the Congo (O'Loughlin et al., 2013). The variation of amplitude in the southern is similar to the
variation observed in the central part, and only a few locations present different behaviors. This is the case, for
instance, of the Lukuga River (bringing water from the Tanganyika Lake to the Lualaba River) that is characterized
by an amplitude lower than 1.5 m, such as some parts of the Kasai basin (upper Kasai, Kwilu and Wamba Rivers) and
some tributaries from the Bateke plateaus. The latters are well known for the stability of their flows, due to a strong
340   groundwater regulation.

Figure 4b-c show the average month for the annual highest and lowest SWH respectively at each VS. The high period
of water levels in the northern sub-basins is September to October, November to December in the central part, and
March to April in the southern part. Conversely, the season of low water levels in the northern sub-basins is March to
April, while the central part of the CRB is at the lowest in May to June with an exception for the Lulonga River and
345   the right bank tributaries upstream the confluence with the Ubangui (e.g., Aruwimi) for which the driest period is
March to April. The Kasaï sub-basin is characterized by two periods of low water levels, September to October and
May to June on the main Kasaï River stem and its other tributaries. Similarly, the major highland Lualaba tributaries
(e.g., Ulindi, Lowa, Elila), fed by the precipitation in the South Kivu region, present lowest levels in May and June.
From its confluence with the Lukuga River and up to Kisangani, the Lualaba River reaches its lowest level in
350   September to October. In the Upemba depression, the low SWH period is November-December. This evidences the
strong seasonal signal of the gradual floods of the CRB, clearly illustrating the influence of rainfall partition in the
northern and southern parts of the basin and the gradual shifts due to the flood travel time along the rivers and
floodplains. This will be further analyzed and discussed in Section 5.

355   **4.1.2 Evaluation of surface water extent characteristics from GIEMS-2**

Figure 5 shows SWE main patterns over the CRB. Figure 5a and b display, respectively, the mean and the mean annual
maximum in the extent of surface water over the 1992-2015 period. Figure 5c shows the variability of SWE, expressed
in terms of the standard deviation over the period. Figure 5d provides the average month of SWE annual maximum
over the record. The figures exhibit very realistic spatial distributions of the major drainage systems, rivers and
360   tributaries (Lualaba, Congo, Ubangui, Kasaï) of CRB. The dataset captures well the associated wetlands and inundated
areas even in regions with complex floodplains, characterized by extensive flooding in the presence of dense
vegetation cover, such as in the *Cuvette Centrale*. Along with the main wetlands in the *Cuvette Centrale*, the Bangwelo
swamps and the valley that contains several lakes (Upemba) are also well delineated. These regions are generally
characterized by a large variability (Fig. 5c) and a great maximum inundation extent (Fig. 5b) especially in the *Cuvette
365   Centrale* and in the Lualaba sub-basin dominated by the presence of large lakes and seasonal floodplains (Becker et
al., 2018). At the basin scale, and in agreement with the results from the altimetry-derived SWH, GIEMS-2 shows that
the *Cuvette Centrale* is flooded at its maximum in October-November (Fig. 5d), while the northern hemisphere part
of the basin reaches its maximum in September-October, and the Kasai and southern eastern part in January-February.

Hydrology and
Earth System
Sciences
Discussions

Open Access

EGU

The spatial distribution of GIEMS-2 SWE was extensively evaluated over Tropical River basins, such as over the

370 Amazon, the Ganges-Brahamaputra and the Mekong. In Prigent et al. (2007) and in Aires et al. (2013), it was compared against SWE from high-resolution (100m) Synthetic Aperture Radar images over high and low water seasons in the Central Amazon (Hess et al., 2003), along with other regional estimates of wetland and open-water distributions (such as the International Geosphere-Biosphere Programme (IGBP) water bodies), leading to an overall estimation of GIEMS uncertainties of ~10 %. Over the entire Tropical band, it was evaluated against the Surface Water Microwave

375 Product Series (SWAMPS, Pham-Duc et al., 2017) along with the Global Lakes and Wetlands Database estimates (Fluet-Chouinard et al., 2015) and Global Surface Water dataset (GSW, Pekel et al., 2016, as in Prigent et al., 2020). Recently, Fatras et al. (2021), see their Fig. 3 and 6 that compared several estimates of SWE over the CRB including L-Band SMOS-derived products (SWAF, Surface WAter Fraction, Parrens et al., 2017) against GSW extent, ESA-CCI (European Space Agency-Climate Change Initiative), and IGBP water bodies products and SWAMPS over the

380 2010–2013 time period, showing an overall similar spatial distribution as observed in GIEMS-2.

Seasonal and interannual variations of the CRB basin-scale total SWE and the associated anomalies over 1992-2015 are shown in Fig. 5e and f. The deseasonalized anomalies are obtained by subtracting the 25-year mean monthly value from each individual month. The total CRB SWE extent shows a strong seasonal cycle (Fig. 5e), with a mean annual averaged maximum of ~65,000 km^2 over the 1992–2015 period with a maximum ~80,000 km^2 in 1998. The time

385 series show a bimodal pattern that characterizes the hydrological annual cycle of the CRB. It also displays a substantial interannual variability especially near the annual maxima. The deseasonalized anomaly in Fig. 5f reveals anomalous events that recently affect the CRB in terms of flood or drought events. As discussed in Becker et al. (2018), the positive Indian Ocean Dipole (pIOD) events in conjunction with the El Niño event that happened in 1997-1998 and 2006-2007 triggered floods in East Africa, Western Indian Ocean, and South India (Mcphaden, 2002; Ummenhofer

390 et al., 2009) and resulted in the large positive peaks observed. The CRB was also impacted by significantly severe and sometimes multi-year droughts during the 1990's and 2000's, impacting often about half of the basin (Ndehedehe et al., 2019). These events can be depicted from GIEMS-2 anomaly time series with repetitive negative signal peaks.

In order to evaluate SWE dynamics at basin and sub-basin scales, here we compare at the monthly time step the

395 seasonal and interannual variabilities of the GIEMS-2 estimates against available in situ water discharge and stages (Table 1).

First, at the entire basin-scale, Fig. 6 displays the comparison between the total area of CRB SWE with the river discharge measured at the Brazzaville/Kinshasa station, the most downstream station available for our study near the mouth of the CRB basin. There is a fair agreement between the interannual variation (Fig. 6a) of the surface water

400 extent and the in situ discharge over the period 1992 to 2015 with a significant coefficient correlation (r = 0.67 with 0 month lag; p-value <0.01) and a fair correlation for its associated anomaly (r = 0.58; p-value <0.01). Both on the raw time series and its anomaly (Fig. 6b), SWE captures major hydrological variations, including the yearly and bimodal peaks. The seasonal comparison (Fig. 6c) shows that the SWE reaches its maximum one month before the maximum of the discharge in December. From January to March, the discharge decreases while the SWE remains high. For the

405 secondary peak, the SWE maximum is reached two months before the one for discharge in May. This is in agreement

with the results shown with the SWE spatial distribution of the average month of the maximum inundation in October-November in the *Cuvette Centrale* (Fig. 5a).

Further, the evaluation of SWE dynamics is performed at the sub-basin level against available observations at the outlets of each of the 5 sub-basins. Similar, to Fig. 6, Fig. 7 shows the comparisons of the aggregated SWE at the

410 sub-basin scale against in situ observations at their respective outlet stations (Bangui for Ubangui, Ouesso for Sangha, Lumbu-Dima for Kasaï, Kisangani for Lualaba, and Brazzaville/Kinshasa for the Middle-Congo sub-basin). For Lualaba and Kasai, in situ SWHs are used since no discharge observation is available. For each sub-basin, we estimate the maximum linear correlation coefficient of point time records between the SWE and the other variables when lagged in time (months). The temporal shift helps to express an estimated travel time of water to reach the basin outlet.

415 There is a general good agreement (with high lagged correlations r >0.8; Fig. 7a, d, g, m) between both variables, and lag time ranging between 0 and 2 months with SWE preceding the discharge, except for the Lualaba. The seasonal analysis in Ubangui and Sangha sub-basins shows that the discharge starts to increase one month prior to SWE (from May), probably related to local precipitation downstream the basins, before both variables increase steadily and reach their maximum in October-November (Fig. 7c and f). For the Kasaï sub-basin (Fig. 7i), SWE increases from July,

420 followed within a month by the water stage, reaching a peak respectively in December and January. While SWE slowly decreases from January, only the discharge continues to increase to reach a maximum in April. For Middle-Congo sub-basin (Fig. 7o), the dynamics of SWE and discharge are in good agreement with the SWE behavior steadily preceding the discharge by one month. The annual dual peak is well depicting the annual dual peak. On the other hand, the Lualaba sub-basin with a moderate correlation (r = 0.54 and lag = 0 month; Fig. 7j) shows a particular behavior

425 with the water stage often preceding the SWE (Fig. 7l). This could be explained by the upstream part of the Lualaba sub-basin which hydrology might be disconnected from the drainage system due to the large seasonal floodplains and lakes, well captured by GIEMS. These water bodies store freshwater and delay its travel time, while the outlet still receives water from other tributaries in the basin. For all sub-basins, the inter-annual deseasonalized anomalies present in general positive and moderate linear correlations (0.4< r <0.5; p-value <0.01 with 0 month lag; Fig. 7b, e, h, k)

430 except for the Middle-Congo where the correlation is greater (0.63; p-value <0.01) with temporal shift of 1 month (Fig. 7n). This confirms the good capabilities of satellite-derived SWE to portray anomalous hydrological events in agreement with in situ observations at the sub-basin scale.

At the basin scale, we have already showed that the annual variability of the CRB discharge is in good agreement with the dynamic of SWE, from seasonal to interannual time scales. Figure 8 investigates the comparison between water

435 flow at Brazzaville/Kinshasa station against the variability of SWE for each sub-basin. For Ubangui, Sangha and Middle-Congo (Fig. 8a, d, g), the variability of water discharge is strongly related to the SWE variations with a respective lag of two, one, and zero months, related to the decreasing distance between the sub-basin and the gauging station. The time series of the anomalies of the above sub-basins capture also some of the large peak variations while other peaks are observed at the sub-basin scale. Kasaï sub-basin presents a good correspondence (r = 0.74 and lag =

440 0) between the water flow and SWE time series and their associated anomaly (r = 0.47 and lag = 0). Unlike the other four sub-catchments, Lualaba presents again a low agreement (r = 0.05 and lag = 0) with, as already seen in Fig. 7, a

non-consistent behavior and shifted variations between SWE and discharge (Fig. 8m), related to lakes and floodplains storage which delay the water transfer to the main river. Nevertheless, anomalies like the strong one in 1998, with large floods linked to a positive Indian Ocean Dipole in conjunction with an El Nino (Becker et al., 2018) are in phase

445   and within same order of magnitude (Fig. 8n).

A focus on the Middle-Congo anomaly time series reveals that it is the only sub-basin where all the variations in the peak discharge are well captured in SWE. This reflects the strong influence of the Middle-Congo floodplains on the flow at Brazzaville/Kinshasa station, which variability may be explained at ~35 % by the variations of SWE in the *Cuvette Centrale,* based on the maximum lagged correlation of 0.59 for the deseasonalized anomalies of the two

450   variables. More interestingly, while the river discharge shows a double peak in its seasonal climatology (a maximum one in December and a secondary one in May), it is not portrayed in the SWE in most sub-basins, except for the Middle-Congo that also receives contributions from Shanga, Ubangui, Kasai and Lualaba. The next section investigates these characteristics.

4.2 A better understanding on how CRB surface water flows

455   The satisfactory behaviour of both SWH from radar altimetry and SWE from GIEMS-2, presented in the previous sections, provides confidence to further analyse the dynamics of surface water and its patterns within the CRB.

Here, we determine the maximum of the linear Pearson correlation (with p-value < 0.1) considering a time lag between the satellite-derived SWH at each VS (from ERS2, ENV, J2/3, SRL and S3A missions) and GIEMS SWE at each cell, against Brazzaville/Kinshasa SWH and discharge, respectively. Note that the temporal shift between SWH/SWE and

460   in situ stages and discharges is constrained between acceptable values, i.e., it cannot be negative, as we are investigating the time needed by surface waters to reach Brazzaville/Kinshasa station. For each VS, the longest possible time series is used. For GIEMS-2, the data over 24-year record are used against the entire river discharge record (1992-2015). The maps of highest correlations and their corresponding time shifts are provided in Fig. 9. Note that both satellite-derived datasets are jointly analysed to support and complement each other individual result. As a

465   validation, the linear Pearson correlation coefficients between altimeter-derived SWH and GIEMS-2 SWE for each location within a 25 km distance and a common availability of data were estimated. The correlations found are very high (>0.9) across the entire CRB.

Figure 9a and b evidence that the northern (Sangha, Ubangui) and the central (western Middle-Congo, downstream tributaries of Kasaï) parts are fairly correlated (r >0.6; p-value <0.1), both in terms of SWH and SWE to the discharge

470   at Brazzaville/Kinshasa. In the eastern part of the Middle Congo and downstream part of the Lualaba River, SWH and SWE show different patterns, with higher maximal correlations for SWH (>0.6) than SWE (<0.5). On the other hand, the south-eastern part of the Lualaba sub-basin presents low correlation (r <0.2) for both variables, confirming again that the discharge at Brazzaville/Kinshasa station is not strongly influenced by the remote water dynamics from the south-eastern part of the CRB. The temporal shifts (in months) associated to the maximum correlation (Fig. 9c and d)

475   at each VS and GIEMS-2 cell (only locations where r ≥0.6 are displayed) help to estimate the water travel time to the Brazzaville/Kinshasa reach. As expected, the time lag for both SWH and SWE increases with the distance from the Brazzaville/Kinshasa station from 0 up to 3 months in remote areas and small tributaries of the upper CRB. The

Hydrology and
Earth System
Sciences
Discussions
Open Access
EGU

mainstream of the Congo in the Middle-Congo sub-basin and northern Kasai are characterized by zero month of lag due to their proximity with the reference station (Brazzaville/Kinshasa). Some left and right-margin tributaries (for

480 instance the Likouala aux Herbes, Dja River) present a one month lag. The Ubangui and Sangha sub-basins show a minimum of two months lag and up to three months for the remote area in the far northern part of the Ubangui basin (Kotto, Bomu rivers, Fig. 9c). Interestingly, on the downstream part of the Ubangui river and in the *Cuvette Centrale*, there is a notable one month difference between the lag in SWH and SWE. While the SWH shows lag time of 0-1 month, it is 1-2 months for SWE. This can be explained by specific hydrological mechanisms of wetlands and large

485 floodplains and the processes between river and floodplains connectivity. These differences can be due in one hand to the different behaviours between water level dynamics and water extent in shallow flooded areas, where SWH in river generally increases before the surface water extent increases with riverbank overflows, while the waters stand for a longer time in the wetlands than in the rivers. The differences might also be attributed to relatively disconnected wetlands and rivers, and/or to the presence of interfluvial wetlands fed directly by local precipitation instead of

490 overbank flooding.

The water travel time through the rivers and sub-basins of CRB were previously investigated by using observations from a few in situ gauges (Bricquet, 1993), while our current study enables a similar analysis at the large scale of the entire CRB.

In order to confirm and validate the results on the dynamics of water surface flows obtained from altimeter-derived

495 SWH and GIEMS-derived SWE, we perform a similar analysis using water level and flow observations from historical (<1994) and current gauges, as presented in Table 2. For each station, covering all the sub-basins considered, we estimated the correlation between the available observations and the observations at Brazzaville/Kinshasa station, at daily and monthly time steps. The results are presented in Table 3. In order to facilitate the comparisons, results for the VSs and SWE cells (as presented in Fig. 9) related to the nearest available in situ gauge stations are reported in

500 Table 3, even if not covering the same period of time.

Overall, the results from the Table 3 supports the general findings reported in Fig. 9, both in terms of optimum coefficient correlation and in terms of lag, with a general good agreement between in situ and satellite observations. The correlation analysis (with p-value <0.05; the change of p-value is related to the in situ record length) between observations at Brazzaville/Kinshasa and the various other stations confirms the higher positive values (r >0.7; with a

505 mean time lag of 8 days and 0 month) with increasing maximum correlation when closest to Brazzaville/Kinshasa in situ station. Lower-Congo also shows very high correlations (r >0.8). Kasaï sub-basin presents low to moderate positive lagged correlation (0.35 to 0.55, lag = 0) with values decreasing with respect to longer distance from the month, in agreement with the results from the satellite estimates. For the Lualaba sub-basin, the results at Kisangani outlet station presents a moderate maximum correlation (r >0.6), similar to the values obtained with SWH from

510 altimetry. In agreement with the results for both SWH and SWE, in situ observations confirm that in other upstream locations of the Lualaba, which are connected to lakes and floodplains, very low linear correlations (r <0.2) are observed. Both Ubangui and Sangha sub-basins have large positive correlations (r >0.7) with a respective time lag of 2 months (65 days) and 1 month (45 days), similar to what satellite observations provided. The difference observed in

515 the correlation coefficient and the lag between SWH and SWE, for the Basoko station in the Middle-Congo for instance, confirms also the different hydrological behavior between the adjacent wetlands and the main river channel. This is also in line with the one month lag observed at some locations in the *Cuvette Centrale* between both satellite derived SWH and SWE, supporting that different processes drive the relation between river channel height and flood extent dynamics.

520 A supplementary analysis was performed in order to better illustrate the spatial distribution of the CRB flood dynamics all over the various tributaries, and also their different timing and how each sub-basin contributes to the peculiar bimodal pattern of the hydrological regime downstream the main stem at Brazzaville/Kinshasa (Fig. 9 and 10). Here, we reproduced the same analysis as above but now considering individually two distinct periods of the year corresponding to each hydrological peak observed at Brazzaville/Kinshasa. We first consider the August-February period (the first large peak) for each time series and estimate the correlation. Then we consider the March-July period 525 corresponding to the secondary peak. The results are shown in Fig. 10 and the comparison/validation of the results with historical and current in situ records are summarized in Table 4.

Figure 10 clearly depicts the relative contributions of northern sub-basins and the southern sub-basins to the first peak and to the second peak, respectively. Regarding the first peak (Fig. 10a, c, e, g), the major contribution of the Ubangui and Sangha rivers (r > 0.6) to the downstream main stem at Brazzaville/Kinshasa during the August-February period 530 is evidenced, with a water transfer time to Brazzaville/Kinshasa station ranging between 1 and 3 months (again, increasing with the distance to the gauging station). Middle-Congo, northern Kasaï and the highland of the Lualaba sub-basins also show some contribution during this period but with 0 to 1 month lag. Water that supplies the second peak of the hydrograph comes essentially from the center and the southern part of the basin (Fig. 10b, d, f), including remote rivers in the Kasai sub-basin with 1-2 months lag and the western part of the Lualaba. The very low correlations 535 between the upper part of the basin (Kivu region, Luapula and upper Lualaba) and discharge at Brazzaville/Kinshasa suggests that the contribution in terms of discharge of this region to the hydrological cycle downstream is negligible, for both peaks, in comparison to that from other tributaries. These conclusions are supported by the similar analyses performed using the in situ observation records (Table 4). This confirms the relatively low contribution of the northern part to the second peak at Brazzaville/Kinshasa station. On the monthly basis, the lags are found similar with the in 540 situ and satellite observations, while the daily data from the in situ records help to get a better characteristic of the travel time at finer time scale. For instance, with the second peak of the hydrograph, the Kasaï and Middle-Congo sub-basins are characterized respectively by a mean time lag of 1 month (28 days) and zero month (7 days) depending on the data sampling interval considered.

545 **5 Conclusion and perspectives**

The present study uses a unique joint analysis of in situ and satellite-derived observations to better characterize CRB surface hydrology and its variability. First, thanks to the availability of an in situ database of historical and contemporary observations of water levels and discharges, we provide an intensive and comprehensive validation of long-term (~25-year) time series from spaceborne water level variations and surface water extent throughout the CRB.

550 The comparison of radar altimetry-derived water levels with in situ water stage at the interannual scale shows an overall good agreement, with standard errors in general lower than 0.30 m. The analysis of the RMSD across the various missions shows an improvement over time from ERS-2 (tens of centimeters) to S3A/B (few centimeters) missions, confirming the technological improvement in terms of sensors, and data processing. A total of more than 2,300 VSs covering the 1995-2020 period was used in this study and is now freely available. When compared to in

555 situ observations, GIEMS-2 SWE also shows consistent and complementary information at the sub-basin and basin scales. These two long-term records are then used to analyze the spatio-temporal dynamics of surface freshwater and its propagation at sub-basin and basin scales, significantly improving our understanding on how surface water flows in the CRB.

The analysis of the large database of SWH from altimetry shows that the amplitude varies greatly across the basin,

560 from more than 5 m in Ubangui and Sangha Rivers, while the *Cuvette Centrale* and the southern basins display smaller annual variations (1.5 m to 4.5 m). The maximum level is reached in September-October in the northern part of the basin, in November-December in the central part and in March-April in the Lualaba region. Surface water bodies and wetlands in the Lualaba sub-basin and *Cuvette Centrale* present the highest variation in extent across the sub-basins and reach their maximum inundation respectively in January-February and November-December. Then we investigate

565 the hydrology contributions and water travel times from upstream to downstream reaches by comparing SWE and SWH to stage and discharge at the Brazzaville/Kinshasa station. In particular, the methodology permitted to better illustrate the spatial distribution of the CRB flood dynamics on the various tributaries, their different timing, and how each sub-basin contributes to the peculiar bimodal pattern of the hydrological regime downstream of the main stem in Brazzaville/Kinshasa. The time shift for both SWH and SWE increases with the distance from the

570 Brazzaville/Kinshasa station from no time lag at the vicinity of the outlet up to 3 months in remote areas and small tributaries of the CRB. Northern sub-basins and the central Congo region highly contribute to the large August-March peak, while the southern part supplies water to both peaks, and in particular to the second one. These results are supported by in situ observations to confirm the findings from satellites observations and from previous studies. Our results therefore confirm the suitability of both long-term water surface elevation time series from radar altimetry and

575 flooded areas from GIEMS-2 for monitoring the CRB surface water dynamics, potentially bridging the gap between past in situ databases and current and future monitoring as an ensemble. Their use in hydrological models will permit a better representation of local and basin-scale hydrodynamics and ensure an improved monitoring of hydrological variables from space.

The very first use of a large dataset of VSs spread over more than a hundred of tributaries across the basin and spanning

580 the whole altimetry period permitted an unprecedented analysis in terms of both length of the observation and number of observations, providing time series of more than twenty years over the CRB. This unique dataset of surface water levels variations combined to the ~25-year SWE from GIEMS should permit to generate estimates of surface water storage. In complement to GRACE/GRACE-FO total water storage estimates, it will further permit the estimation of long-term and interannual variations of freshwater volume in the CRB, including subsurface and groundwater storage

585 and their link with hydro-climatic processes across the region. Furthermore, the use of both satellite datasets in hydrological models will permit a better representation of local and basin-scale hydrodynamics and ensure an

improved real-time monitoring of hydrological variables from space, as well as a better evaluation of climate variability impacts on water availability. These datasets will also play a key role in the evaluation and validation of future hydrology-oriented satellite missions such as the NASA-CNES Surface Water and Ocean Topography (SWOT),

590 to be launched in late 2022. More generally, the use of satellite-derived observations dedicated to surface hydrology will contribute to a better fundamental understanding of CRB and its hydro-climatic processes, bringing more opportunities for other river basins in Africa to improve the management of water resources.

Finally, the better understanding of large-scale CRB surface hydrology variability will help to improve the comprehension at the local and regional scales of the hydrological and biogeochemical cycles, as CRB is recognized

595 to be one of the three main convective centers in the tropics and its inland waters strongly contribute to the carbon cycle of the basin. Our findings also highlight the large spatio-temporal variability of the surface hydrologic components within the basin that will help understand the links and feedback with regional climate and the influence of events such as El Niño on water resources. The results from both long term SWH from radar altimetry and flooded areas from GIEMS-2 have confirmed the benefits of EO in characterizing and understanding the variability of the

600 surface hydrologic components in a sparse gauged basin such as CRB. Since these datasets are global, our study and the methodology will benefit to similar investigations in other ungauged tropical river basins.

Figure captions

Figure 1 Congo River Basin (CRB): its topography from Multi-Error-Removed Improved-Terrain (MERIT) digital elevation model, major sub-basins (in brown line), major rivers and tributaries. Also displayed are the locations of in

620 situ gauging stations (triangle). Red and black triangles represent respectively the gauge stations with current (>1994) and historical observations. Their characteristics are reported in Table 1.

Figure 2 Locations of altimetry VSs over time within the CRB. (a) ERS-2 VSs covering the 1995-2002 period. (b) ENV, ENV2, J2 and SRL VSs during 2002-2016. (c) J3, S3A and S3B VSs from 2016 up to present. (d) VSs with

625 actual long time series from combination of multi-satellite missions with the record period ranges between 25 to 20
years (yellow), 20 to 15 years (orange), and 15 to 10 years (red).

Figure 3 Comparison of in situ water stage (Table 1) and altimeter-derived SWH at different sites (Fig. 1 for their
locations). The left panel presents the time series of both in situ and altimetry-derived water height where the grey
line in the background shows the in situ daily WS variations (grey), the sky-blue line indicates the in situ WS sampled
at the same date as the altimeter-derived SWH from ERS-2 (purple), ENV (royal blue), ENV2 (lime green), SRL (dark
630 orange), J2/3 (yellow), and S3A/S3B (red) missions. The middle panel shows the histogram of the difference between
the altimeter derived SWH and the in situ WS. The right panel portrays the scatterplot between altimeter derived SWH
and in situ WS. The linear correlation coefficient r and the Root-Mean-Square Deviation (RMSD) considering all the
observations are indicated. The solid line shows the linear regression between both variables.

Figure 4 Statistics for radar altimetry VSs. (a) displays the maximum amplitude of SWH (in m), (b) presents the
635 average month of the maximum of SWH, and (c) shows the average month of the minimum of SWH.

Figure 5 Characterization of SWE from GIEMS-2 over the CRB. (a) Mean SWE (1992-2015) for each pixel,
expressed in percentage of the pixel coverage size of 773 km^2. (b) SWE variability (standard deviation over 1992-
2015, also in %). (c) Annual maximum SWE averaged over 1992-2015 (in %). (d) Monthly mean SWE for 1992–
2015 for the entire CRB. (e) Time series of SWE, and (f) Corresponding deseasonalized anomalies obtained by
640 subtracting the 24 years mean monthly value from individual months.

Figure 6 Comparison of monthly SWE (a) and its anomalies (b) at CRB scale against the in situ monthly mean water
discharge at Brazzaville/Kinshasa station. The blue line is the SWE, and the green line is the mean water discharge.
(c) the annual cycle for both variables (1992-2015), with the shaded areas illustrating the standard deviations around
the SWE and discharge means.

645 **Figure 7** Similar to Fig. 6 but for each of the 5 sub-basins. Comparison of monthly SWE (absolute and anomaly
values) against the in situ water discharge or SWH at each sub-basin outlet. The blue line is for the SWE and the green
line is for the water discharge (Ubangui, Sangha, Middle-Congo) or the water stage (Kasai, Lualaba). The annual
cycle for both variables (1992-2015) is also displayed, with the shaded areas illustrating the standard deviations around
SWE and discharge means.

650 **Figure 8** Similar to Fig. 6 and 7, but the SWE estimated at each of the 5 sub-basins is compared against the in situ
monthly mean water discharge at Brazzaville/Kinshasa station. The blue line is for the SWE and the green line is for
the at Brazzaville/Kinshasa station. The annual cycle for each variable (1992-2015) is also displayed, with the shaded
areas illustrating the standard deviations around the SWE and discharge means.

Figure 9 Maps of the optimal coefficient correlation and associated lag at each VS and GIEMS-2 cells. (a) Optimum
655 coefficient correlation between altimetry-derived SWH (from ERS2, ENV, SRL, J2/3 and S3A missions) at each VS
against in situ water stage at the Brazzaville/Kinshasa station. (b) Same as (a) for each GIEMS-2 cell against the river

discharge at Brazzaville/Kinshasa station. (c) and (d) show, respectively, their optimum lag in months. In (c) and (d), only the time lags for which the maximum correlation has p-value <0.05 are displayed.

Figure 10 Similar to Fig. 9 but considering the two distinct periods of the year corresponding to each hydrological
660 peak observed at Brazzaville/Kinshasa. (a) the optimum coefficient correlation between altimetry-derived SWH (from ERS2, ENV, SRL, J2/3 and S3A missions) at each VS against in situ water stage at the Brazzaville/Kinshasa station for the period August-February (b) same as (a) but for the period March-July. (c) the optimum coefficient correlation between SWE at each GIEMS-2 against in situ discharge at the Brazzaville/Kinshasa station for the period August-February. (d) same as (c) but for the period March-July. (e), (f), (g) show the time lag (in month) associated
665 respectively to (a), (b) and (c), only for cases where the maximum correlation has p-value <0.05. The time lag associated to (d) has too few values with p-value <0.05 and is not shown.

References

670 Aires, F., Papa, F., and Prigent, C.: Along-term, high-resolution wetland dataset over the Amazon basin, downscaled from a multiwavelength retrieval using SAR data, J. Hydrometeor., 14, 594–607, doi:10.1175/JHM-D-12-093.1, 2013.

Aloysius, N., and Saiers, J.: Simulated hydrologic response to projected changes in precipitation and temperature in the Congo River basin, Hydrol. Earth Syst. Sci., 21, 4115–4130, https://doi.org/https://doi.org/10.5194/hess-21-
675   4115-2017, 2017.

Alsdorf, D., Beighley, E., Laraque, A., Lee, H., Tshimanga, R., O'Loughlin, F., Mahé, G., Dinga, B., Moukandi, G., and Spencer, R. G. M.: Opportunities for hydrologic research in the Congo Basin. Rev. Geophys., 54, 378–409, https://doi.org/10.1002/2016RG000517, 2016.

Andriambeloson, J. A., Paris, A., Calmant, S., and Rakotondraompiana, S.: Re-initiating depth-discharge monitoring
680   in small-sized ungauged watersheds by combining remote sensing and hydrological modelling: a case study in Madagascar, Hydrol. Sci. J., 65, 2709-2728, DOI: 10.1080/02626667.2020.1833013, 2020.

Becker, M., Papa, F., Frappart, F., Alsdorf, D., Calmant, S., da Silva, J. S., Prigent, C., and Seyler, F.: Satellite-based estimates of surface water dynamics in the Congo River Basin, Int. J. Appl. Earth Obs. Geoinf., 66, 196–209, https://doi.org/10.1016/j.jag.2017.11.015, 2018.

685 Becker, M., Santos, J., Calmant, S., Robinet, V., Linguet, L., and Seyler, F.: Water Level Fluctuations in the Congo Basin Derived from ENVISAT Satellite Altimetry, Remote sens., *6*, 9340–9358, https://doi.org/10.3390/rs6109340, 2014.

Bele, Y., Mulotwa, E., Bokoto de Semboli, B., Sonwa, D., and Tiani, A. : Afrique centrale: Les effets du changement

Hydrology and
Earth System
Sciences
Discussions
Open Access
EGU

climatique dans le Bassin du Congo: la nécessité de soutenir les capacités adaptatives locales, CRDI/CIFOR,
690   Canada, 5pp., 2010.

Betbeder, J., Gond, V., Frappart, F., Baghdadi, N. N., Briant, G., and Bartholomé, E.: Mapping of Central Africa
forested wetlands using remote sensing, IEEE J. Sel. Top. Appl. Earth Obs. Remote Sens., 7, 531-542,
10.1109/JSTARS.2013.2269733, 2014.

Bogning, S., Frappart, F., Blarel, F., Niño, F., Mahé, G., Bricquet, J. P., Seyler, F., Onguéné, R., Etamé, J., Paiz, M.
695   C., and Braun, J. J.: Monitoring water levels and discharges using radar altimetry in an ungauged river basin:
The case of the Ogooué. Remote Sens., 10, 350, https://doi.org/10.3390/rs10020350, 2018.

Bonnefond, P., Verron, J., Aublanc, J., Babu, K., Bergé-Nguyen, M., Cancet, M., Chaudhary, A., Crétaux, J.-F.,
Frappart, F., Haines, B., et al. The Benefits of the Ka-Band as Evidenced from the SARAL/AltiKa
AltimetricMission: Quality Assessment and Unique Characteristics of AltiKa Data, Remote Sens., 10, 83,
700   https://doi.org/10.3390/rs10010083, 2018.

Burnett, M., Quetin, G., and Konings, A.: Data-driven estimates of evapotranspiration and its drivers in the Congo
Basin, Hydrol. Earth Syst. Sci., 24, 4189–4211., https://doi.org/10.5194/hess-2020-186, 2020.

Bricquet, J. P.: Les Ecoulements Du Congo a Brazzaville Et La Spatialisation Des Apports, in: Grands Bassins
Fluviaux Péri-Atlantiques : Congo, Niger, Amazone, Paris (FRA), 22-24 Novembre 1993, 27-38, 1993.

705 Bwangoy, J. R. B., Hansen, M. C., Roy, D. P., De Grandi, G., and Justice, C. O.: Wetland mapping in the Congo Basin
using optical and radar remotely sensed data and derived topographical indices, Remote Sens. Environ., 114,
73-86, 2010.

Carr, A. B., Trigg, M. A., Tshimanga, R. M., Borman, D. J., and Smith, M. W.: Greater water surface variability
revealed by new Congo River field data: Implications for satellite altimetry measurements of large rivers,
710   Geophys. Res. Lett., 46, 8093–8101. https://doi.org/10.1029/2019GL083720, 2019.

Corbari, C., Huber, C., Yesou, H., Huang, Y., and Su, Z.: Multi-Satellite Data of Land Surface Temperature, Lakes
Area, and Water Level for Hydrological Model Calibration and Validation in the Yangtze River Basin, Water,
11, 2621, https://doi.org/10.3390/w11122621, 2019.

Cretaux, J., Frappart, F., Papa, F., Calmant, S., Nielsen, K., and Benveniste, J.: Hydrological Applications of Satellite
715   Altimetry Rivers, Lakes, Man-Made Reservoirs, Inundated Areas, in: Satellite Altimetry over Oceans and Land
Surfaces, edited by: Stammer, D. C. and Cazenave, A., Taylor & Francis Group, New York, 459-504, 2017.

Crowhurst, D., Dadson, S., Peng, J., and Washington, R.: Contrasting controls on Congo Basin evaporation at the two
rainfall peaks, Clim. Dyn., 56, 1609–1624, https://doi.org/10.1007/s00382-020-05547-1, 2021.

Dargie, G. C., Lewis, S. L., Lawson, I. T., Mitchard, E. T. A., Page, S. E., Bocko, Y. E., and Ifo, S. A.: Age, extent
720   and carbon storage of the central Congo Basin peatland complex, Nature, 542, 86–90,

https://doi.org/10.1038/nature21048, 2017.

Datok, P., Fabre, C., Sauvage, S., Moukandi N'kaya, G. D., Paris, A., Dos Santos, V., Guilhen, J., Manteaux S,
Laraque, A., and Sanchez Perez, J. M.: Investigating the role of the Cuvette Centrale wetlands in the hydrology,
sediment and carbon fluxes of the Congo River Basin (CRB). Earth Sp. Sci. Open Arch., 43,
725   https://doi.org/https://doi.org/10.1002/essoar.10505504.1, 2020.

Da Silva, J., Calmant, S., Seyler, F., Corrêa, O., Filho, R., Cochonneau, G., and João, W.: Water levels in the Amazon
basin derived from the ERS 2 and ENVISAT radar altimetry missions, Remote Sens. Environ., 114, 2160–2181,
https://doi.org/10.1016/j.rse.2010.04.020, 2010.

Decharme, B., Alkama, R., Papa, F., Faroux, S., Douville, H., and Prigent, C.: Global off-line evaluation of the ISBA-
730   TRIP flood model, Clim. Dyn., *38*, 1389–1412, https://doi.org/10.1007/s00382-011-1054-9, 2011.

Decharme, B., Douville, H., Prigent, C., Papa, F., and Aires, F.: A new river flooding scheme for global climate
applications: Off-line evaluation over South America, J. Geophys. Res. Atmos., 113, 1–11,
https://doi.org/10.1029/2007JD009376, 2008.

Fan, L., Wigneron, J.-P., Ciais, P., Chave, J., Brandt, M., Fensholt, R., Saatchi, S. S., Bastos, A., Al-Yaari, A.,
735   Hufkens, K., Qin, Y., Xiao, X., Chen, C., Myneni, R. B., Fernandez-Moran, R., Mialon, A., Rodriguez-
Fernandez, N. J., Kerr, Y., Tian, F., and Penuelas, J.: Satellite-observed pantropical carbon dynamics, Nat.
Plants, 5, 944–951, https://doi.org/10.1038/s41477-019-0478-9, 2019.

Fatras, C., Parrens, M., Peña Luque, S., and Al Bitar, A.: Hydrological Dynamics of the Congo Basin From Water
Surfaces Based on L-Band Microwave, Water Resour. Res., 57, https://doi.org/10.1029/2020wr027259, 2021.

740   Fluet-Chouinard, E., Lehner, B., Rebelo, L. M., Papa, F., and Hamilton, S. K.: Development of a global inundation
map at high spatial resolution from topographic downscaling of coarse-scale remote sensing data, Remote Sens.
Environ., 158, 348–361, doi:10.1016/j.rse.2014.10.015, 2015.

Frappart, F., Papa, F., Famiglietti, J. S., Prigent, C., Rossow, W. B., and Seyler, F.: Interannual variations of river
water storage from a multiple satellite approach: A case study for the Rio Negro River basin, J. Geophys. Res.,
745   113, 1–12, https://doi.org/10.1029/2007JD009438, 2008.

Frappart, F., Papa, F., Güntner, A., Werth, S., Ramillien, G., Prigent, C., Rossow, W. B., and Bonnet, M. P.:
Interannual variations of the terrestrial water storage in the lower ob' basin from a multisatellite approach,
Hydrol. Earth Syst. Sci., 14, 2443–2453, https://doi.org/10.5194/hess-14-2443-2010, 2010.

Frappart, F., Calmant, S., Cauhopé, M., Seyler, F., and Cazenave, A.: Preliminary results of ENVISAT RA-2-derived
750   water levels validation over the Amazon basin, Remote Sens. Environ., 100, 252–264,
https://doi.org/10.1016/j.rse.2005.10.027, 2006.

Frappart, F., Papa, F., Malbeteau, Y., León, J. G., Ramillien, G., Prigent, C., Seoane, L., Seyler, F., and Calmant, S.:

Surface freshwater storage variations in the Orinoco floodplains using multi-satellite observations, Remote Sens., 7, 89–110, https://doi.org/10.3390/rs70100089, 2015.

755   Frappart, F., Papa, F., Marieu, V., Malbeteau, Y., Jordy, F., Calmant, S., Durand, F. and Bala, S.: Preliminary assessment of SARAL/AltiKa observations over the Ganges-Brahmaputra and Irrawaddy Rivers, Mar. Geod., 38, 568-580, https://doi.org/10.1080/01490419.2014.990591, 2015.

Frappart, F., Legrésy, B., Nino, F., Blarel, F., Fuller, N., Fleury, Birol, S. F., and Calmant, S.: An ERS-2 altimetry reprocessing compatible with ENVISAT for long-term land and ice sheets studies. Remote Sens. Environ., 184, 760   558-581, https://doi.org/10.1016/j.rse.2016.07.037, 2016.

Garambois, P. A., Calmant, S., Roux, H., Paris, A., Monnier, J., Finaud-Guyot, P., Samine Montazem, A., and da Silva, J. S.: Hydraulic visibility: Using satellite altimetry to parameterize a hydraulic model of an ungauged reach of a braided river, Hydrol. Process., 31, 756–767, https://doi.org/10.1002/hyp.11033, 2017.

Hastenrath, S.: Climate and circulation of the tropics, D. Reidel Publishing Company, Holland, 1985.

765   Hess, L. L., Melack, J. M., Novo, E., Barbosa, C., and Gastil, M.: Dual-season mapping of wetland inundation and vegetation for the central Amazon basin, Remote Sens. Environ., 87, 404–428, doi:10.1016/j.rse.2003.04.001, 2003.

Hua, W., Zhou, L., Chen, H., Nicholson, S. E., Raghavendra, A., and Jiang, Y.: Possible causes of the Central Equatorial African long-term drought Possible causes of the Central Equatorial African long-term drought, 770   Environ. Res. Lett., 11, 124002, https://doi.org/10.1088/1748-9326/11/12/124002, 2016.

Ingram, V., Tieguhong, J. C., Schure, J., Nkamgnia, E., and Tadjuidje, M. H.: Where artisanal mines and forest meet: Socio-economic and environmental impacts in the Congo Basin, Nat. Resour. Forum, 35, 304–320, https://doi.org/10.1111/j.1477-8947.2011.01408.x, 2011.

Inogwabini, B-I.: The changing water cycle: Freshwater in the Congo, WIREs Water, 7, e1410, 775   https://doi.org/10.1002/wat2.1410, 2020.

Kao, H., Kuo, C., Tseng, K., Shum, C. K., Tseng, T.-P., Jia, Y.-Y., Yang, T.-Y., Ali, T. A., Yi, Y., and Hussain, D.: Assessment of Cryosat-2 and SARAL / AltiKa altimetry for measuring inland water and coastal sea level variations: A case study on Tibetan Plateau Lake and Taiwan Coast, Mar. Geod., 42, 327–343, https://doi.org/10.1080/01490419.2019.1623352, 2019.

780   Kittel, C. M. M., Jiang, L., Tøttrup, C., and Bauer-Gottwein, P.: Sentinel-3 radar altimetry for river monitoring - A catchment-scale evaluation of satellite water surface elevation from Sentinel-3A and Sentinel-3B, Hydrol. Earth Syst. Sci., 25, 333–357, https://doi.org/10.5194/hess-25-333-2021, 2021.

Laraque, A., Bellanger, M., Adele, G., Guebanda, S., Gulemvuga, G., Pandi, A., Paturel, J. E., Robert, A., Tathy, J. P., and Yambele, A.: Evolutions récentes des débits du Congo, de l'Oubangui et de la Sangha, Geo-Eco-Trop,

785   37, 93–100, 2013.

Laraque, Alain, Bricquet, J. P., Pandi, A., and Olivry, J. C.: A review of material transport by the Congo River and its
          tributaries, Hydrol. Process., 23, 3216–3224, https://doi.org/10.1002/hyp.7395, 2009.

Laraque, Alain, N'kaya, G. D. M., Orange, D., Tshimanga, R., Tshitenge, J. M., Mahé, G., Nguimalet, C. R., Trigg,
          M. A., Yepez, S., and Gulemvuga, G.: Recent budget of hydroclimatology and hydrosedimentology of the congo
790   river in central Africa, Water, 12, 2613, https://doi.org/10.3390/w12092613, 2020.

Lee, H., Beighley, R. E., Alsdorf, D., Chul, H., Shum, C. K., Duan, J., Guo, J., Yamazaki, D., and Andreadis, K.:
          Remote Sensing of Environment Characterization of terrestrial water dynamics in the Congo Basin using
          GRACE and satellite radar altimetry, Remote Sens. Environ., 115, 3530–3538,
          https://doi.org/10.1016/j.rse.2011.08.015, 2011.

795   Leon, J. G., Calmant, S., Seyler, F., Bonnet, M. P., Cauhopé, M., Frappart, F., Filizola, N., and Fraizy, P.: Rating
          curves and estimation of average water depth at the upper Negro River based on satellite altimeter data and
          modeled discharges, J. Hydrol., 328, 481–496, https://doi.org/10.1016/j.jhydrol.2005.12.006, 2006.

Loughlin, F. O., Trigg, M. A., Schumann, G. J., and Bates, P. D.: Hydraulic characterization of the middle reach of
          the Congo River, Water Resour. Res., 49, 5059–5070, https://doi.org/10.1002/wrcr.20398, 2013.

800   Mcphaden, M. J.: El Nino and La Nina : Causes and Global Consequences, in: Encyclopedia of Global Environmental
          Change, edited by: MacCracken, M. C. and Perry, J. S., United States of America, 353–370, 2002.

Moreira, D. M., Calmant, S., Perosanz, F., Xavier, L., Rotunno Filho, O. C., Seyler, F., and Monteiro, A. C.:
          Comparisons of observed and modeled elastic responses to hydrological loading in the Amazon basin, Geophys.
          Res. Lett., 43, 9604–9610, doi:10.1002/2016GL070265, 2016.

805   Munzimi, Y. A., Hansen, M. C., and Asante, K. O.: Estimating daily streamflow in the Congo Basin using satellite-
          derived data and a semi-distributed hydrological model, Hydrol. Sci. J., 64, 1472–1487,
          https://doi.org/10.1080/02626667.2019.1647342, 2019.

Ndehedehe, C. E., Anyah, R. O., Alsdorf, D., Agutu, N. O., and Ferreira, V. G.: Modelling the impacts of global multi-
          scale climatic drivers on hydro-climatic extremes (1901 – 2014) over the Congo basin, Sci. Total Environ., 651,
810   1569–1587, https://doi.org/10.1016/j.scitotenv.2018.09.203, 2019.

Ndehedehe, C. E., Awange, J. L., Agutu, N. O., and Okwuashi, O.: Changes in hydro-meteorological conditions over
          tropical West Africa (1980 – 2015) and links to global climate, Glob. Planet. Change, 162, 321–341,
          https://doi.org/10.1016/j.gloplacha.2018.01.020, 2018.

Nogherotto, R., Coppola, E., Giorgi, F., and Mariotti, L.: Impact of Congo Basin deforestation on the African
815   monsoon, Atmos. Sci. Lett., 14, 45–51, https://doi.org/10.1002/asl2.416, 2013.

Normandin, C., Frappart, F., Diepkilé, A. T., Marieu, V., Mougin, E., Blarel, F., Lubac, B., Braquet, N., and Ba, A.:

Evolution of the performances of radar altimetry missions from ERS-2 to Sentinel-3A over the Inner Niger Delta, Remote Sens., 10, 833, https://doi.org/10.3390/rs10060833, 2018.

O'Loughlin, F. ., Neal, J., Schumann, G. J., Beighley, R. E., and Bates, P. D.: A LISFLOOD-FP hydraulic model of
820   the middle reach of the Congo, J. Hydrol., 580, 124203, https://doi.org/https://doi.org/10.1016/j.jhydrol.2019.124203, 2019.

OMM.: CONGO-HYCOS, Organisation météorologique mondiale, 101 pp., https://library.wmo.int/doc_num.php?explnum_id=4883, 2010.

Paiva, R. C. D. de, Buarque, D. C., Collischonn, W., Bonnet, M., Frappart, F., Calmant, S., and Mendes, C. A. B.:
825   Large-scale hydrologic and hydrodynamic modeling of the Amazon River basin, Water Resour. Res., 49, 1226–1243, https://doi.org/10.1002/wrcr.20067, 2013.

Papa, F, Gu, A., Frappart, F., Prigent, C., and Rossow, W. B.: Variations of surface water extent and water storage in large river basins: A comparison of different global data sources, Geophys. Res. Lett., 35, 1–5, https://doi.org/10.1029/2008GL033857, 2008.

830   Papa, F., Prigent, C., Aires, F., Jimenez, C., Rossow, W. B., and Matthews, E.: Interannual variability of surface water extent at the global scale, 1993-2004, J. Geophys. Res. Atmos., 115, 1–17, https://doi.org/10.1029/2009JD012674, 2010.

Papa, F., Bala, S. K., Pandey, R. K., Durand, F., Gopalakrishna, V. V, Rahman, A., and Rossow, W. B.: Ganga-Brahmaputra river discharge from Jason-2 radar altimetry: An update to the long-term satellite-derived estimates
835   of continental freshwater forcing flux into the Bay of Bengal, J. Geophys. Res., 117, C11021, https://doi.org/10.1029/2012JC008158, 2012.

Papa, F., Frappart, F., Güntner, A., Prigent, C., Aires, F., Getirana, A. C. V., and Maurer, R.: Surface freshwater storage and variability in the Amazon basin from multi-satellite observations, 1993-2007, J. Geophys. Res. Atmos., 118, 11,951-11,965, https://doi.org/10.1002/2013JD020500, 2013.

840   Papa, F., Frappart, F., Malbeteau, Y., Shamsudduha, M., Vuruputur, V., Sekhar, M., Ramillien, G., Prigent, C., Aires, F., Pandey, R. K., Bala, S., and Calmant, S.: Satellite-derived surface and sub-surface water storage in the Ganges-Brahmaputra River Basin, J. Hydrol. Reg. Stud., 4, 15–35, https://doi.org/10.1016/j.ejrh.2015.03.004, 2015.

Paris, A, Calmant, S., Gosset, M., Fleischmann, A., Conchy, T., and Garambois, P.: Monitoring hydrological variables
845   from remote sensing and modelling in the Congo River basin, Earth Sp. Sci. Open Arch., 53, https://doi.org/10.1002/essoar.10505518.1, 2020.

Paris, Adrien, De Paiva, R. D., Da Silva, J. S., Moreira, D. M., Calmant, S., Garambois, P.-A., Collischonn, W., Bonnet, M., and Seyler, F.: Stage-discharge rating curves based on satellite altimetry and modeled discharge in the Amazon basin, Water Resour. Res., 52, 3787–3814, https://doi.org/10.1002/2014WR016618.Received,

850   2016.

Park, E.: Characterizing channel- fl oodplain connectivity using satellite altimetry: Mechanism, hydrogeomorphic
control, and sediment budget, Remote Sens. Environ., 243, 111783, https://doi.org/10.1016/j.rse.2020.111783,
2020.

Parrens, M., Al Bitar, A., Frappart, F., Papa, F., Wigneron, J.-P., and Kerr, Y.: Mapping dynamic water fraction under
855   the tropical rain forests of the Amazonian basin from L-band brightness temperature, Water, 9, 350,
https://doi.org/10.3390/w9050350, 2017.

Pekel, J.-F., A. Cottam, N. Gorelick, and Belward, A. S.: High-resolution mapping of global surface water and its
long-term changes, Nature, 540, 418–422, doi:10.1038/nature20584, 2016.

Pham-Duc, B., Prigent, C., and Aires, F.: Surface water monitoring within Cambodia and the Vietnamese Mekong
860   Delta over a year, with Sentinel-1 SAR observations. Water, 9, 366, https://doi.org/10.3390/w9060366, 2017.

Plisnier, P. D., Nshombo, M., Mgana, H., and Ntakimazi, G.: Monitoring climate change and anthropogenic pressure
at Lake Tanganyika, J. Great Lakes Res., 44, 1194–1208, https://doi.org/10.1016/j.jglr.2018.05.019, 2018.

Prigent, C., Jimenez, C., and Bousquet, P.: Satellite-Derived Global Surface Water Extent and Dynamics Over the
Last 25 Years (GIEMS-2), J. Geophys. Res. Atmos., 125, 1–21, https://doi.org/10.1029/2019JD030711, 2019.

865   Prigent, Catherine, Papa, F., Aires, F., Rossow, W. B., and Matthews, E.: Global inundation dynamics inferred from
multiple satellite observations, 1993-2000, J. Geophys. Res. Atmos., 112, 1993–2000,
https://doi.org/10.1029/2006JD007847, 2007.

Pujol, L., Garambois, P. A., Finaud-Guyot, P., Monnier, J., Larnier, K., Mosé, R., Biancamaria, S., Yesou, H., Moreira,
D., Paris, A., and Calmant, S.: Estimation of multiple inflows and effective channel by assimilation of multi-
870   satellite hydraulic signatures: The ungauged anabranching Negro river, J. Hydrol., 591, 125331,
https://doi.org/10.1016/j.jhydrol.2020.125331, 2020.

Raney, R. K.: The delay/Doppler radar altimeter, IEEE Trans. Geosci. Remote Sens., 36, 1578-1588, doi:
10.1109/36.718861, 1998.

Ringeval, B., De Noblet-Ducoudré, N., Ciais, P., Bousquet, P., Prigent, C., Papa, F., and Rossow, W. B.: An attempt
875   to quantify the impact of changes in wetland extent on methane emissions on the seasonal and interannual time
scales, Global Biogeochem. Cycles, 24, https://doi.org/10.1029/2008GB003354, 2010.

Rosenqvist, Å., and Birkett, C. M.: Evaluation of JERS-1 SAR mosaics for hydrological applications in the Congo
River basin, Int. J. Remote Sens., 23, 1283-1302, https://doi.org/10.1080/01431160110092902, 2002.

Runge, J.: The Congo River, Central Africa, in: Large Rivers: Geomorphology and Management, Gupta, A., John
880   Wiley and Sons, 293–309, https://doi.org/10.1002/9780470723722.ch14, 2007.

Seyler, F., Calmant, S., Silva, J., Filizola, N., Roux, E., Cochonneau, G., Vauchel, P., and Bonnet, M.: Monitoring water level in large trans-boundary ungauged basins with altimetry: the example of ENVISAT over the Amazon basin, in: 6th SPIE Asia Pacific Remote Sensing Conference, Nouméa, France, November 2008, 10.1117/12.813258, 2008.

885 Stammer, D., and Cazenave, A.: Satellite Altimetry over Oceans and Land Surfaces, Taylor and Francis Group, Boca Raton, London, New York, 645 pp., 2017.

Sun, W., Ishidaira, H., and Bastola, S.: Calibration of hydrological models in ungauged basins based on satellite radar altimetry observations of river water level, Hydrol. Process., 26, 3524–3537, https://doi.org/10.1002/hyp.8429, 2012.

890 Tshimanga, R.M., and Hughes, D.A.: Climate change and impacts on the hydrology of the Congo Basin: the case of the northern sub-basins of the Oubangui and Sangha Rivers, Phys. Chem. Earth, 50–52, 72–83, https://doi.org/10.1016/j.pce.2012.08.002, 2012.

Tshimanga, R. M., and Hughes, D. A.: Basin-scale performance of a semi-distributed rainfall-runoff model for hydrological predictions and water resources assessment of large rivers: the Congo River, Water Resour. Res., 895 50, 1174–1188, https://doi.org/10.1002/2013WR014310.Received, 2014.

Tshimanga, R.M., Hughes, D. A., and Kapangaziwiri, E.: Initial calibration of a semi-distributed rainfall runoff model for the Congo River basin, Phys. Chem. Earth, 36, 761–774, https://doi.org/10.1016/j.pce.2011.07.045, 2011.

Tshimanga, R.M.: Two decades of hydrologic modeling and predictions in the Congo River Basin: Progress and prospect for future investigations, Under press, in: Congo Basin Hydrology, Climate, and Biogeochemistry: A 900 Foundation for the Future, edited by: Alsdorf, D., Tshimanga, R.M, and Moukandi, G. N., Wiley-AGU, ISBN "9781119656975", 2021.

Ummenhofer, C. C., England, M. H., Mcintosh, P. C., Meyers, G. A., Pook, M. J., Risbey, J. S., and Gupta, A. S., and Taschetto, A. S.: What causes southeast Australia's worst droughts?, Geophys. Res. Lett., 36, https://doi.org/10.1029/2008GL036801, 2009.

905 Verhegghen, A., Mayaux, P., De Wasseige, C., and Defourny, P.: Mapping Congo Basin vegetation types from 300 m and 1 km multi-sensor time series for carbon stocks and forest areas estimation, Biogeosciences, 9, 5061–5079, https://doi.org/10.5194/bg-9-5061-2012, 2012.

Zakharova, E., Nielsen, K., Kamenev, G., and Kouraev, A.: River discharge estimation from radar altimetry: Assessment of satellite performance, river scales and methods, J. Hydrol., 583, 124561, 910 https://doi.org/10.1016/j.jhydrol.2020.124561, 2020.
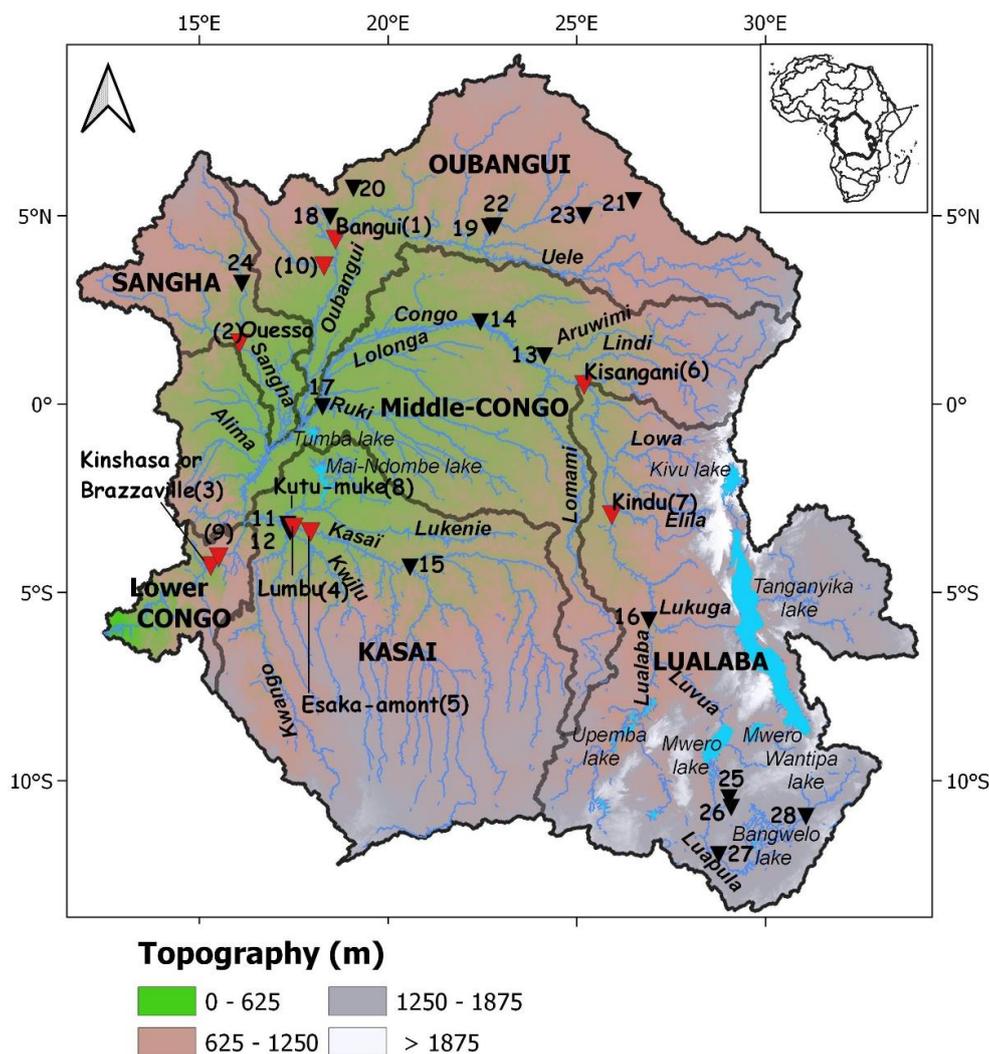
Figure 1 Congo River Basin (CRB): its topography from Multi-Error-Removed Improved -Terrain (MERIT) digital elevation model, major sub-basins (in brown line), major rivers and tributaries. Also displayed are the locations of in situ gauging stations (triangle). Red and black triangles represent respectively the gauge stations with current (>1994) and historical observations. Their characteristics are reported in Table 1.

915
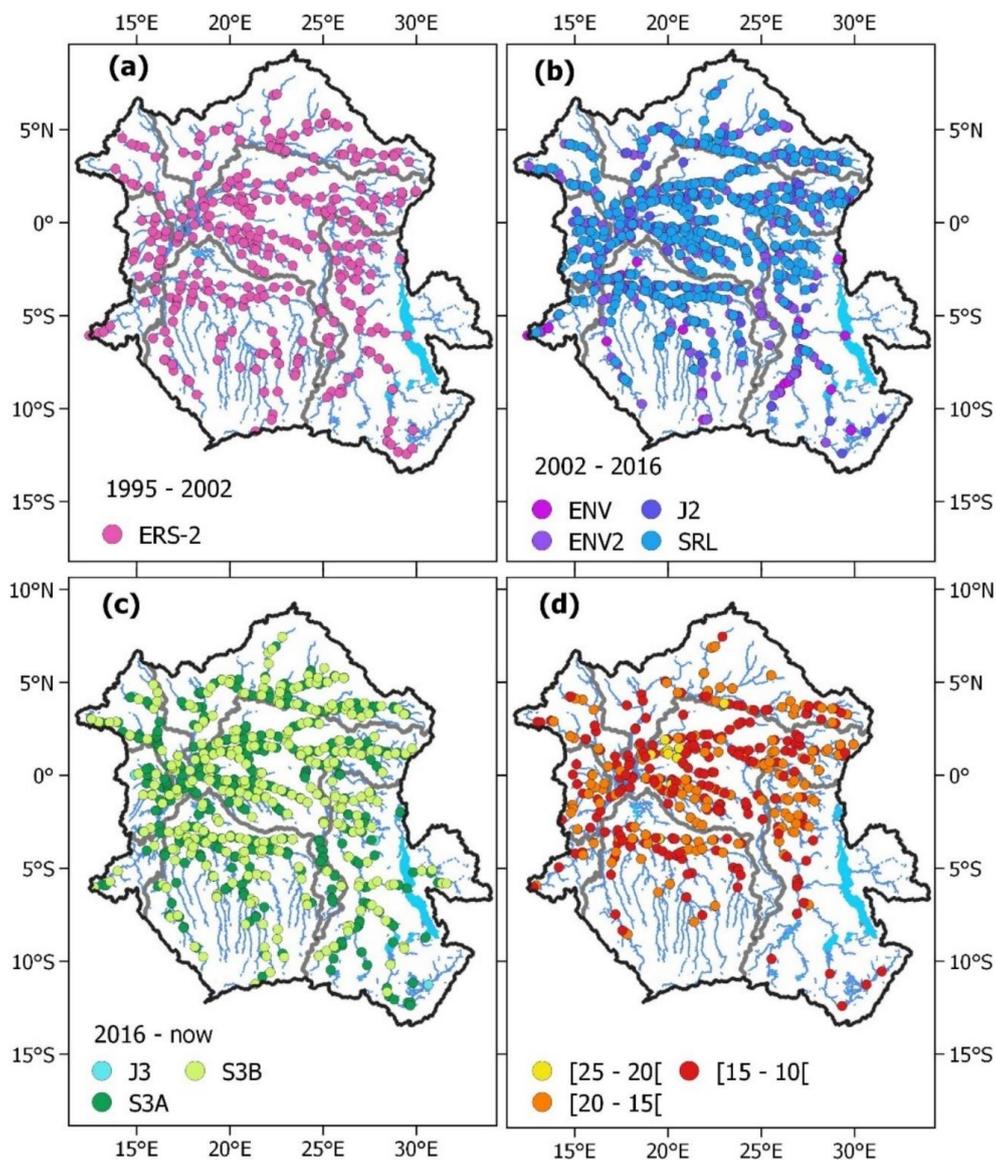
920

Figure 2 Locations of altimetry VSs over time within the CRB. (a) ERS-2 VSs covering the 1995-2002 period. (b) ENV, ENV2, J2 and SRL VSs during 2002-2016. (c) J3, S3A and S3B VSs from 2016 up to present. (d) VSs with actual long time series from combination of multi-satellite missions with the record period ranges between 25 to 20 years (yellow), 20 to 15 years (orange), and 15 to 10 years (red).

925

Figure 3 Comparison of in situ water stage (Table 1) and altimeter-derived SWH at different sites (Fig. 1 for their locations). The left panel presents the time series of both in situ and altimetry-derived water height where the grey line in the background shows the in situ daily WS variations (grey), the sky-blue line indicates the in situ WS sampled at the same date as the altimeter-derived SWH from ERS-2 (purple), ENV (royal blue), ENV2 (lime green), SRL (dark orange), J2/3 (yellow), and S3A/S3B (red) missions. The middle panel shows the histogram of the difference between the altimeter derived SWH and the in situ WS. The right panel portrays the scatterplot between altimeter derived SWH and in situ WS. The linear correlation coefficient r and the Root-Mean-Square Deviation (RMSD) considering all the observations are indicated. The solid line shows the linear regression between both variables.

930
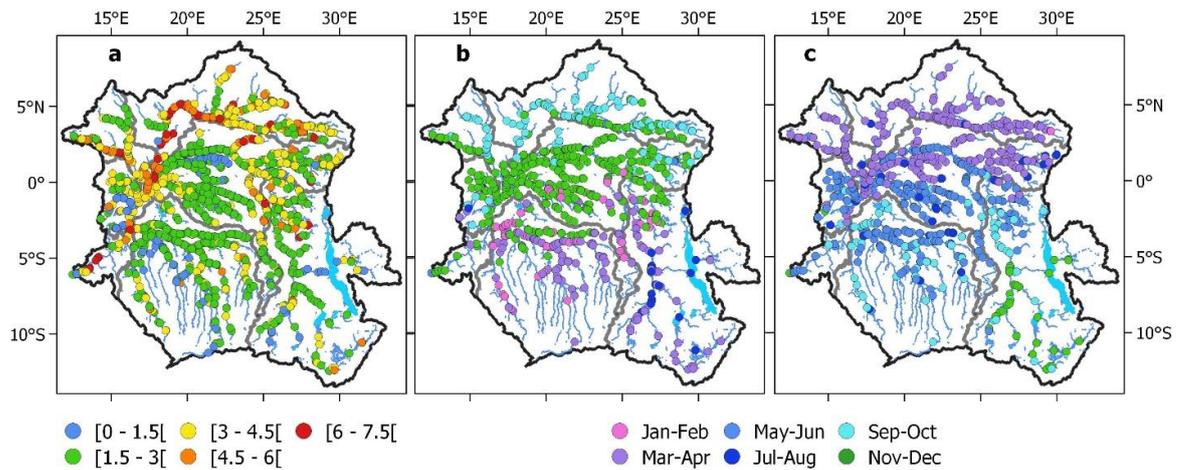
935

940

945

Figure 4 Statistics for radar altimetry VSs. (a) displays the maximum amplitude of SWH (in m), (b) presents the average month of the maximum of SWH, and (c) shows the average month of the minimum of SWH.
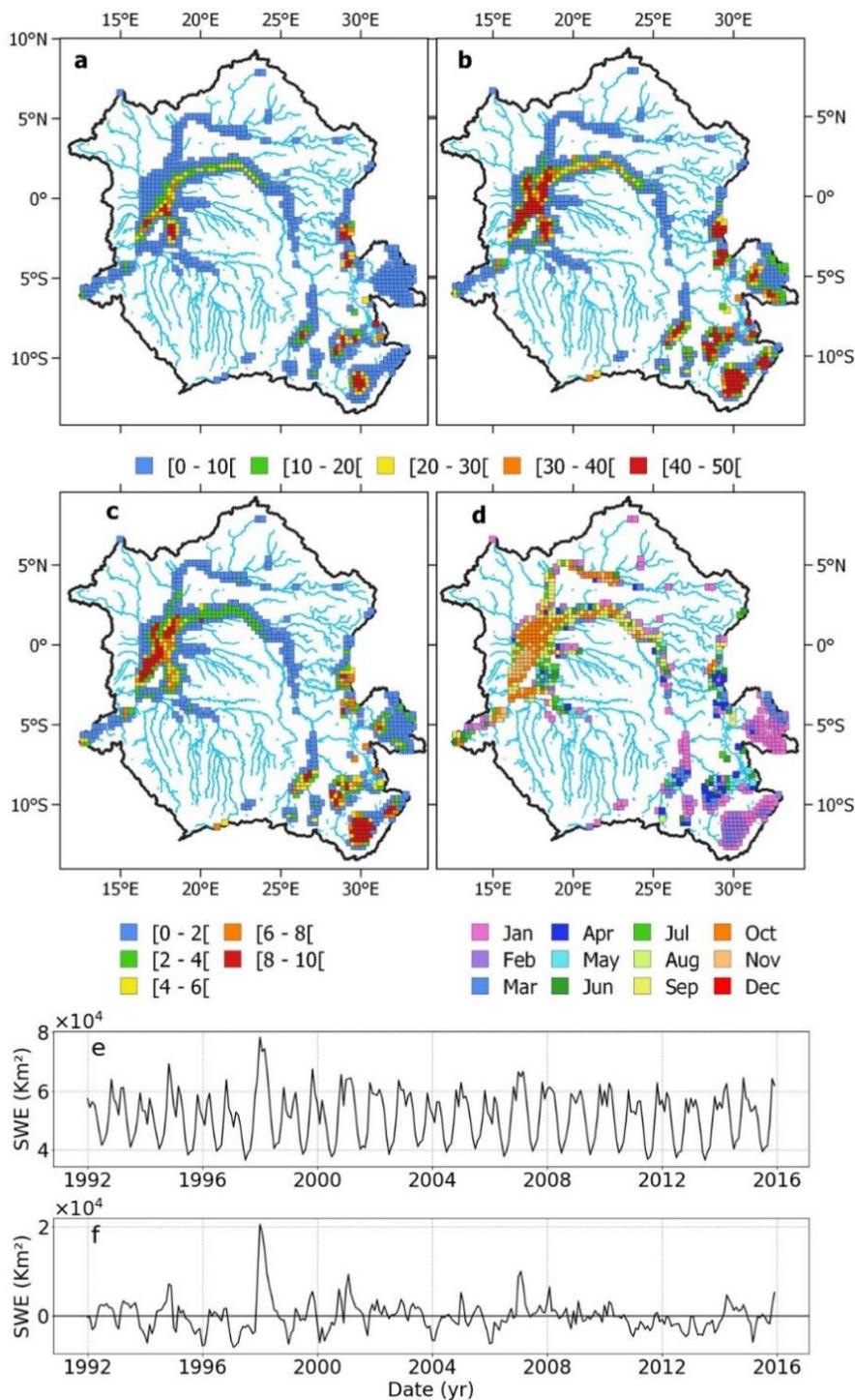
950

Figure 5 Characterization of SWE from GIEMS-2 over the CRB. (a) Mean SWE (1992-2015) for each pixel, expressed in percentage of the pixel coverage size of 773 km^2. (b) SWE variability (standard deviation over 1992-2015, also in %). (c) Annual maximum SWE averaged over 1992-2015 (in %). (d) Monthly mean SWE for 1992–2015 for the entire CRB. (e) Time series of SWE, and (f) Corresponding deseasonalized anomalies obtained by subtracting the 24 years mean monthly value from individual months.

955

960

965

970

975

Figure 6 Comparison of monthly SWE (a) and its anomalies (b) at CRB scale against the in situ monthly mean water discharge at Brazzaville/Kinshasa station. The blue line is the SWE, and the green line is the mean water discharge. (c) the annual cycle for both variables (1992-2015), with the shaded areas illustrating the standard deviations around the SWE and discharge means.

Figure 7 Similar to Fig. 6 but for each of the 5 sub-basins. Comparison of monthly SWE (absolute and anomaly values) against the in situ water discharge or SWH at each sub-basin outlet. The blue line is for the SWE and the green line is for the water discharge (Ubangui, Sangha, Middle-Congo) or the water stage (Kasai, Lualaba). The annual

985 cycle for both variables (1992-2015) is also displayed, with the shaded areas illustrating the standard deviations around SWE and discharge means.

Figure 8 Similar to Fig. 6 and 7, but the SWE estimated at each of the 5 sub-basins is compared against the in situ monthly mean water discharge at Brazzaville/Kinshasa station. The blue line is for the SWE and the green line is for the at Brazzaville/Kinshasa station. The annual cycle for each variable (1992-2015) is also displayed, with the shaded areas illustrating the standard deviations around the SWE and discharge means.

Figure 9 Maps of the optimal coefficient correlation and associated lag at each VS and GIEMS-2 cells. (a) Optimum coefficient correlation between altimetry-derived SWH (from ERS2, ENV, SRL, J2/3 and S3A missions) at each VS against in situ water stage at the Brazzaville/Kinshasa station. (b) Same as (a) for each GIEMS-2 cell against the river discharge at Brazzaville/Kinshasa station. (c) and (d) show, respectively, their optimum lag in months. In (c) and (d), only the time lags for which the maximum correlation has p-value <0.05 are displayed.

Figure 10 Similar to Fig. 9 but considering the two distinct periods of the year corresponding to each hydrological peak observed at Brazzaville/Kinshasa. (a) the optimum coefficient correlation between altimetry-derived SWH (from ERS2, ENV, SRL, J2/3 and S3A missions) at each VS against in situ water stage at the Brazzaville/Kinshasa station for the period August-February (b) same as (a) but for the period March-July. (c) the optimum coefficient correlation between SWE at each GIEMS-2 against in situ discharge at the Brazzaville/Kinshasa station for the period August-February. (d) same as (c) but for the period March-July. (e), (f), (g) show the time lag (in month) associated respectively to (a), (b) and (c), only for cases where the maximum correlation has p-value <0.05. The time lag associated to (d) has too few values with p-value <0.05 and is not shown.

Table 1 Location and main characteristics of in situ stations used in this study. The locations are displayed in Fig. 1.
WS: Water Stage.

N°	Name	Lat	Lon	Sub-basin	Variable	Period	Frequency	Source
Stations with contemporary observations								
1	Bangui	4.37	18.61	Ubangui	ws/ Discharge	1936-2020	Daily/Monthly	CRREBaC/ SO-Hybam
2	Ouesso	1.62	16.07	Sangha	ws/ Discharge	1947-2020	Daily/Monthly	CRREBaC/ SO-Hybam
3	Brazzaville/ Kinshasa	-4.3	15.30	Lower-Congo	ws/ Discharge	1903-2020	Daily/Monthly	CRREBaC/ SO-Hybam
4	Lumbu-dima	-3.28	17.5	Kasaï	ws	1909-2012	Daily	CRREBaC
5	Esaka-amont	-3.4	17.94	Kasaï	ws	1977-2010	Daily	CRREBaC
6	Kisangani	0.51	25.19	Lualaba	ws/ Discharge	1967-2011/ 1950-1959	Daily/Monthly	CRREBaC
7	Kindu	-2.95	25.93	Lualaba	ws/ Discharge	1960-2004/ 1933-1959	Daily/Monthly	CRREBaC
8	Kutu-muke	-3.20	17.34	Kasaï	Surface water elevation	2017-2020	Hourly	CRREBaC
9	Maluku-Trechot	-4.07	15.51	Lower-Congo	ws	2017-2020/ 1966-1991	Hourly/Daily	CRREBaC
10	Mbata	3.67	18.30	Ubangui	ws/ Discharge	2016-2018/ 1950-1994	Hourly/ Monthly	CRREBaC
Stations with historical observations								
11	Bagata	-3.39	17.40	Kasaï	ws	1952-1990	Daily	CRREBaC
12	Bandundu	-3.30	17.37	Kasaï	ws	1929-1993	Daily	CRREBaC
13	Basoko	1.28	24.14	Middle-Congo	ws	1972-1991	Daily	CRREBaC
14	Bumba	2.18	22.44	Middle-Congo	ws	1912-1961	Daily	CRREBaC
15	Ilebo	-4.33	20.58	Kasaï	ws	1924-1991	Daily	CRREBaC
16	Kabalo	-5.74	26.91	Lualaba	ws	1975-1990	Daily	CRREBaC
17	Mbandaka	-0.07	18.26	Middle-Congo	ws	1913-1984	Daily	CRREBaC
18	Bossele-bali	4.98	18.46	Ubangui	Discharge	1957-1994	Monthly	CRREBaC
19	Bangassou	4.73	22.82	Ubangui	Discharge	1986-1994	Monthly	CRREBaC
20	Sibut	5.73	19.08	Ubangui	Discharge	1951-1991	Monthly	CRREBaC

21	Obo	5.4	26.5	Ubangui	Discharge	1985-1994	Monthly	CRREBaC
22	Loungoumba	4.7	22.69	Ubangui	Discharge	1987-1994	Monthly	CRREBaC
23	Zemio	5.0	25.2	Ubangui	Discharge	1952-1994	Monthly	CRREBaC
24	Salo	3.2	16.12	Sangha	Discharge	1953-1994	Monthly	CRREBaC
25	n.a.	-10.46	29.03	Lualaba	Discharge	1971-2004	Monthly	CRREBaC
26	n.a.	-10.71	29.09	Lualaba	Discharge	1971-2005	Monthly	CRREBaC
27	Chembe Ferry	-11.97	28.76	Lualaba	Discharge	1956-2005	Daily/Monthly	GRDC/ CRREBaC
28	Old pontoon	-10.95	31.07	Chambeshi	Discharge	1972-2004	Daily	GRDC

1020

1025

1030

1035

1040   **Table 2** RMSD and r per satellite missions for each in situ station related to fig. 3.

N°	In situ station	ERS-2		ENV		ENV2		J2/3		SRL		S3A		S3B	
		RMSD (m)	r	RMSD (m)	r	RMSD (m)	r	RMSD (m)	r	RMSD (m)	r	RMSD (m)	r	RMSD (m)	r
1	Bangui	0.46	0.99	0.15	0.99	/	/	/	/	0.23	0.99	/	/	0.42	0.99
2	Ouesso	0.75	0.91	0.32	0.96	0.89	0.89	/	/	0.20	0.99	0.17	0.99	/	/
3	Brazzaville	0.66	0.87	0.33	0.95	/	/	/		0.21	0.99	0.24	0.99	/	/
4	Lumbu-d.	0.30	0.92	0.23	0.96	/	/	0.20	0.96	/	/	/	/	/	/
6	Kisangani	0.40	0.95	0.39	0.94	0.64	0.94	/	/	/	/	/	/	/	/
7	Kindu	/	/	0.27	0.95	/	/	/	/	/	/	/	/	/	/
8	Kutu-mu.	/	/	/	/	/	/	/	/	/	/	0.28	0.98	/	/
9	Maluku_T.	/	/	/	/	/	/	/	/	/	/	0.13	0.99	/	/
10	Mbata	/	/	/	/	/	/	/	/	/	/	0.10	0.98	/	/

1045

1050

1055

43

Table 3 Optimal coefficient correlation and associated lag for each in situ station against SWH and discharge at the Brazzaville/Kinshasa station and their closest VS and GIEMS-2 cell (SWE) and their latitude and longitude in square bracket. In parenthesis, r and lag at the daily time scale when daily observations are available. Only correlations with

1060   a 95% significance are reported.

N°	In situ	Monthly (Daily)	
		r	lag
Kasaï sub-basin			
4	Lumbu-D	0.46 (0.46)	0 (0)
	VS [-3.26, 17.46]	0.48	0
5	Esaka-A	0.34 (0.35)	0 (0)
	VS [-3.40, 18.09]	0.5	0
11	Bagata	0.55 (0.54)	0 (0)
	VS [-3.39, 17.40]	0.66	0
	SWE [-3.38, 17.40]	0.49	0
15	Ilebo	0.40 (0.40)	0 (0)
	VS [-4.34, 20.49]	0.42	0
	SWE [-4.38, 20.68]	0.48	0
Middle-Congo sub-basin			
13	Basoko	0.72 (0.73)	0 (10)
	VS [1.26, 23.72]	0.83	1
	SWE [1.38, 23.88]	0.24	0
14	Bumba	0.72 (0.73)	0 (10)
	VS [2.19, 22.19]	0.78	0
	SWE [2.12, 22.39]	0.51	1
17	Mbandaka	0.92 (0.92)	0 (5)
	VS [-0.04, 18.40]	0.94	0
	SWE [-0.12, 18.38]	0.83	1
Lower-Congo sub-basin			
9	Maluku	0.97 (0.96)	0 (0)
	VS [-4.15, 15.41]	0.97	0
	SWE [-4.12, 15.42]	0.85	0
Lualaba sub-basin			
6	Kisangani	0.64 (0.61)	0 (0)
	VS [0.36, 25.38]	0.63	0
	SWE [0.38, 25.38]	0.39	3
7	Kindu	0.12 (0.13)	0 (0)
	VS [-3.14, 25.93]	0.17	0
	SWE [-2.88, 25.91]	0.32	0
16	Kabalo	-0.17 (-0.17)	3 (0)
	VS [-5.76, 26.91]	-0.3	0
	SWE [-6.38, 27.04]	0.03	0
25	15933300	0.42	1
	VS [-10.68, 28.68]	-0.21	0
26	1593210	0.42	2
	VS [-10.68, 28.68]	-0.21	0
27	1593100	0.55	1
	VS [-11.89, 28.53]	-0.34	0
28	Old pontoon	-0.23 (0.1)	0 (0)
	VS [-10.56, 31.46]	-0.17	0
	SWE [-10.88, 31.19]	0.03	0

	Ubangui sub-basin		
1	Bangui	0.79 (0.78)	2 (65)
	VS [4.35, 18.57]	0.83	2
	SWE [4.38, 18.68]	0.68	2
10	Mbata	0.71	2
	VS [3.66, 18.29]	0.81	2
18	Bossele-Bali	0.53	2
	VS [4.43, 18.34]	0.83	2
19	Bangassou	0.78	2
	VS [4.72, 22.80]	0.78	2
21	Obo	0.65	2
	VS [5.15, 26.30]	0.73	2
22	Loungoumba	0.64	2
	VS [4.81, 22.93]	0.87	2
23	Zemio	0.70	2
	VS [4.90, 24.78]	0.88	2
	Sangha sub-basin		
2	Ouesso	0.69 (0.71)	1 (45)
	VS [1.44, 16.20]	0.81	1
	SWE [0.62, 16.62]	0.61	1
24	Salo	0.78	2
	VS [2.88, 16.24]	0.80	2

1065

1070

1075

Table 4 Optimal coefficient correlation and associated lag for each in situ station against SWH and discharge at the Brazzaville/Kinshasa station for the two periods of time corresponding to the first and second peak and for their closest VS and GIEMS-2 cell (SWE). Their latitude and longitude are in square bracket. In parenthesis, r and lag using daily observations. Only correlations with a 95% significance are reported.

N°	In situ	Peak-1 (August-February)		Peak-2 (March-July)	
		Monthly (Daily)		Monthly (Daily)	
		r	lag	r	lag
Kasaï sub-basin					
4	Lumbu-D	0.63 (0.63)	0 (0)	0.65 (0.63)	1 (30)
	VS [-3.26, 17.46]	0.67	0	0.65	1
5	Esaka-A	0.52 (0.52)	0 (0)	0.52 (0.38)	0 (25)
	VS [-3.40, 18.09]	0.64	0	0.49	1
11	Bagata	0.65 (0.65)	0 (0)	0.57 (0.56)	1 (20)
	VS [-3.39, 17.40]	0.77	0	0.70	0
	SWE [-3.38, 17.40]	0.55	0	0.34	1
15	Ilebo	0.59 (0.59)	0 (0)	0.59 (0.60)	1 (40)
	VS [-4.34, 20.49]	0.66	0	0.64	1
	SWE [-4.38, 20.68]	0.54	0	0.44	2
Middle-Congo sub-basin					
13	Basoko	0.77 (0.81)	1 (15)	0.81 (0.77)	0 (5)
	VS [1.26, 23.72]	0.82	2	0.77	1
	SWE [1.38, 23.88]	0.45	0	0.17	3
14	Bumba	0.77 (0.80)	0 (15)	0.77 (0.77)	0 (10)
	VS [2.19, 22.19]	0.80	0	0.80	0
	SWE [2.12, 22.39]	0.54	1	0.02	3
17	Mbandaka	0.92 (0.93)	0 (5)	0.92 (0.91)	0 (0)
	VS [-0.04, 18.40]	0.96	0	0.84	0
	SWE [-0.12, 18.38]	0.84	1	0.63	0
Lower-Congo sub-basin					
9	Maluku	0.97 (0.97)	0 (0)	0.92 (0.92)	0 (0)
	VS [-4.15, 15.41]	0.97	0	0.90	0
	SWE [-4.12, 15.42]	0.90	0	0.60	1
Lualaba sub-basin					
6	Kisangani	0.83 (0.78)	0 (0)	0.73 (0.77)	0 (0)
	VS [0.36, 25.38]	0.75	0	0.75	0
	SWE [0.38, 25.38]	0.55	3	0.25	3
7	Kindu	0.25 (0.26)	0 (0)	0.66 (0.68)	0 (0)
	VS [-3.14, 25.93]	0.29	0	0.80	0
	SWE [-2.88, 25.91]	0.23	0	0.30	3
16	Kabalo	-0.28 (-0.30)	0 (0)	0.73 (0.74)	0 (0)
	VS [-5.76, 26.91]	-0.18	0	0.81	0
	SWE [-6.38, 27.04]	-0.09	2	0.26	0
28	Old pontoon	(0.22)	(0)	0.60 (0.56)	1 (30)
	VS [-10.56, 31.46]	/	/	0.65	1
	SWE [-10.88, 31.19]	-0.03	3	0.21	0
Ubangui sub-basin					
1	Bangui	0.87 (0.87)	2 (55)	0.23 (0.24)	3 (75)
	VS [4.35, 18.57]	0.82	2	0.41	3
	SWE [4.38, 18.68]	0.6	2	0.05	3
10	Mbata	0.62	2	/	/

	VS [3.66, 18.29]	0.82	2	/	/
18	Bossele-Bali	0.51	3	/	/
	VS [4.43, 18.34]	0.82	2	/	/
19	Bangassou	0.81	2	/	/
	VS [4.72, 22.80]	0.76	2	/	/
21	Obo	0.58	2	/	/
	VS [5.15, 26.30]	/	/	/	/
22	Loungoumba	0.54	2	/	/
	VS [4.81, 22.93]	0.92	2	/	/
23	Zemio	0.65	2	/	/
	VS [4.90, 24.78]	0.91	2	/	/
Sangha sub-basin					
2	Ouesso	0.73 (0.78)	1 (40)	0.28 (0.30)	0 (20)
	VS [1.44, 16.20]	0.81	1	0.35	3
	SWE [0.62, 16.62]	0.63	1	0.17	3
24	Salo	0.81	2	/	/
	VS [2.88, 16.24]	0.78	2	/	/

1080